Sensitivity kernels for coda-wave interferometry and scattering tomography: theory and numerical evaluation in two-dimensional anisotropically scattering media

Ludovic Margerin, Thomas Planès, Jessie Mayor, Marie Calvet

Geophysical Journal International

Geophys. J. Int. (2016) **204,** 650–666 doi: 10.1093/gji/ggv470
GJI Seismology

Sensitivity kernels for coda-wave interferometry and scattering tomography: theory and numerical evaluation in two-dimensional anisotropically scattering media

Ludovic Margerin,[1] Thomas Planès,[2] Jessie Mayor[1] and Marie Calvet[1]

[1] *Institut de Recherche en Astrophysique et Planétologie, Observatoire Midi-Pyrénées, Université Paul Sabatier, C.N.R.S.,* 14 *Avenue Edouard Belin, Toulouse, France. E-mail: Ludovic.Margerin@irap.omp.eu*
[2] *Center for Wave Phenomena, Department of Geophysics, Colorado School of Mines,* 1500 *Illinois Street, Golden, CO* 80401*, USA*

Accepted 2015 October 27. Received 2015 October 16; in original form 2015 May 7

SUMMARY

Coda-wave interferometry is a technique which exploits tiny waveform changes in the coda to detect temporal variations of seismic properties in evolving media. Observed waveform changes are of two kinds: traveltime perturbations and distortion of seismograms. In the last 10 yr, various theories have been published to relate either background velocity changes to traveltime perturbations, or changes in the scattering properties of the medium to waveform decorrelation. These theories have been limited by assumptions pertaining to the scattering process itself—in particular isotropic scattering, or to the propagation regime—single-scattering and/or diffusion. In this manuscript, we unify and extend previous results from the literature using a radiative transfer approach. This theory allows us to incorporate the effect of anisotropic scattering and to cover a broad range of propagation regimes, including the contribution of coherent, singly scattered and multiply scattered waves. Using basic physical reasoning, we show that two different sensitivity kernels are required to describe traveltime perturbations and waveform decorrelation, respectively, a distinction which has not been well appreciated so far. Previous results from the literature are recovered as limiting cases of our general approach. To evaluate numerically the sensitivity functions, we introduce an improved version of a spectral technique known as the method of 'rotated coordinate frames', which allows global evaluation of the Green's function of the radiative transfer equation in a finite domain. The method is validated through direct pointwise comparison with Green's functions obtained by the Monte Carlo method. To illustrate the theory, we consider a series of scattering media displaying increasing levels of scattering anisotropy and discuss the impact on the traveltime and decorrelation kernels. We also consider the related problem of imaging variations of scattering properties based on intensity perturbations observed in the coda. The impact of anisotropy is particularly pronounced for the scattering and decorrelation sensitivity kernels, which probe spatial/temporal changes in the scattering properties of the medium. Compared to the isotropic case, scattering anisotropy strongly increases the sensitivity of coda waves in the vicinity of the single-scattering ellipse, which may have important implications for imaging applications. In addition to demonstrating the impact of non-isotropic scattering on the sensitivity kernels of coda waves, our work offers a practical solution to model this process accurately.

Key words: Seismic tomography; Theoretical seismology; Wave scattering and diffraction.

1 INTRODUCTION

The seismic coda is composed of waves scattered by Earth inhomogeneities (Aki 1969; Aki & Chouet 1975), and has been traditionally used to infer the scattering and absorption properties of the lithosphere (see Sato *et al.* 2012, for a comprehensive review). More recently, thanks to the rapid development of the Green's function reconstruction technique using ambient noise, waveform changes in the coda have been exploited to monitor and characterize temporal variations in active regions, such as volcanoes and fault zones (see Brenguier *et al.* 2011; Sens-Schönfelder & Wegler 2011, for reviews). One of the interesting aspects of the mapping problem lies in the fact that the medium properties can display large lateral variations at different scales. For instance, at scale lengths ranging from a few tens of kilometres to a few

hundred kilometres, it has been observed that the rate of decay of coda waves depends strongly on the geological environment (e.g. Mitchell & Cong 1998; Carcolé & Sato 2010; Calvet *et al.* 2013). At scales of a few kilometres to a few tens of kilometres, irregular coda decay as well as traveltime changes of coda waves have been observed in the vicinity of active seismic faults (e.g. Nishigami 2000; Wegler & Sens-Schönfelder 2007; Brenguier *et al.* 2008a; Chen *et al.* 2010; Nakata & Snieder 2011; Yu & Hung 2012; Froment *et al.* 2013). In addition, continuous seismic monitoring of active volcanoes has revealed that traveltimes changes observed in the coda are strongly dependent on the propagation path between source and station, thereby suggesting medium variations at a scale of a few hundred metres or even less (e.g. Sens-Schönfelder & Wegler 2006; Brenguier *et al.* 2008b; Sens-Schönfelder *et al.* 2014). Finally, it has recently been shown experimentally, numerically and theoretically that the distortion of waveforms observed in the coda could be used to locate and characterize temporal variations of mechanical properties in an evolving medium (Larose *et al.* 2010; Planès *et al.* 2015). This approach has been applied with success to the detection of medium changes preceding/accompanying volcanic eruptions (Obermann *et al.* 2013a). Therefore, whether this pertains to the static or dynamic mapping of Earth's heterogeneities, there is an interest in developing a unified theory of coda-wave sensitivity for observables, such as intensity, waveform decorrelation, or traveltime changes in realistic media.

The key to carry out this task lies in an accurate description of energy transport from source to receiver. In highly scattering media, where polarization and anisotropy are being washed out very rapidly compared to the typical detection time in the coda, the diffusion equation is a simple and efficient transport model. Numerous applications to the mapping of velocity changes in evolving media have been developed. However, in more weakly scattering media the intensity distribution can be highly anisotropic and the diffusion approximation breaks down. In particular, in the vicinity of the source, there is always a part of the energy which propagates ballistically, in sharp contrast with the physical assumptions underlying the diffusion approach. As recently put forward by Mayor *et al.* (2014) in the context of seismology, an accurate physical modeling of coda-wave observables requires the knowledge of the full energy distribution in phase space (ω, t, $\mathbf{r}$, $\mathbf{n}$), where ω is the central frequency of the signal, t is the lapse time in the coda, $\mathbf{r}$ is the position vector and $\mathbf{n}$ is a unit vector indicating the propagation direction of the waves. This distribution is known in the physical literature as the specific intensity $I(\mathbf{r}, t, \mathbf{n})$. More precisely, the amount of energy (per unit frequency) flowing across an oriented surface $d\mathbf{S}$ during time dt in direction $\mathbf{n}$ is given by: $dE = I(\mathbf{r}, t, \mathbf{n})\mathbf{n} \cdot d\mathbf{S}dt$ (see e.g. Chandrasekhar 1960). In practice, the signal is filtered in a narrow frequency band $[\omega, \omega + \delta\omega[$ with $\delta\omega/\omega \ll 1$. As explained in Section 3 ('Green's function calculation'), the specify intensity satisfies a radiative transfer (or transport equation) in a scattering and absorbing medium. From now on, the frequency dependence of the specific intensity will be implicitly assumed. The radiative transfer approach has been adopted in many fields, including atmospheric optics, ultrasonics, medical imaging with I-R light and astrophysics, where scattering effects are important. We refer the interested reader to the review paper of Margerin (2005) or the monograph of Sato *et al.* (2012) for seismological applications.

In this paper, we use basic concepts of radiative transfer theory to derive heuristically two basic coda-wave sensitivity functions. Our treatment emphasizes the difference between medium changes that modify the propagation paths between source and receiver, versus changes that do not. The former (respectively latter) situation corresponds to an active (respectively passive) perturbation. Although the two scenarios are of course idealizations of the true impact of a medium change, it is conceptually important to distinguish between them. Using the (positive-definite) passive and active sensitivity kernels, we calculate the perturbation of key observables which may be employed to image temporal/spatial variations in the Earth using coda waves. In imaging applications, either a diffusion or isotropic scattering approximation has been employed so far. While in volcanic regions the isotropic scattering model has shown good agreement with the data (Yamamoto & Sato 2010), the effect of scattering anisotropy may be much more pronounced in the crust (e.g. Hoshiba 1995; Gusev & Abubakirov 1996; Takahashi *et al.* 2009; Calvet *et al.* 2013). Therefore, an extension of the concept of sensitivity functions to this case appears worthwhile. To address this problem, we introduce a spectral technique to evaluate the Green's function of the radiative transfer equation. This allows us to describe accurately the angular dependence of the specific intensity in anisotropically scattering media. This spectral method is used to approximate numerically the sensitivity kernels for three important observables: traveltime shifts, decorrelation of waveforms and intensity perturbations. The first two observables can be employed to detect *temporal* changes of the medium, while the latter probes spatial variation of scattering properties. The theory is illustrated with a series of 2-D numerical examples, which demonstrate the influence of coherent propagation and scattering anisotropy on the spatial dependence of coda-wave sensitivities.

2 SENSITIVITY FUNCTIONS

In this section, we introduce two basic sensitivity functions for coda-wave tomography. The first one may be termed 'passive' and describes all possible paths between source and receiver which visit an arbitrary small control volume in a scattering medium (see Fig. 1). It can be viewed as an extension of the sensitivity function introduced by Pacheco & Snieder (2005) in the framework of diffusion theory. The second one may be termed 'active' in the sense that it quantifies the effect of new propagation paths which are generated by a local perturbation of the scattering properties in the medium (see Planès *et al.* 2014; Mayor *et al.* 2014,and Fig. 1). By combining the 'passive' and 'active' kernels, it is possible to derive sensitivity functions for the relevant observables in the seismic coda.

Let us consider a point source and a receiver located at $\mathbf{r}_0$ and $\mathbf{r}$, respectively. We denote by $G(\mathbf{r}, t, \mathbf{n}; \mathbf{r}_0, \mathbf{n}_0)$ the probability for a 'seismic phonon' (a term coined by Shearer & Earle 2004) leaving the source in direction $\mathbf{n}_0$ at time $t = 0$ to arrive at the receiver at time t in direction $\mathbf{n}$. This probability density function can be physically interpreted as the specific intensity generated by an impulsive and mono-directional unit source acting at $\mathbf{r}_0$. Hereafter, we always assume excitation by a unit source which allows us to use directly the specific intensity as an expression of probability. If we are not interested in the particular direction in which the phonon reaches the receiver, we may introduce the

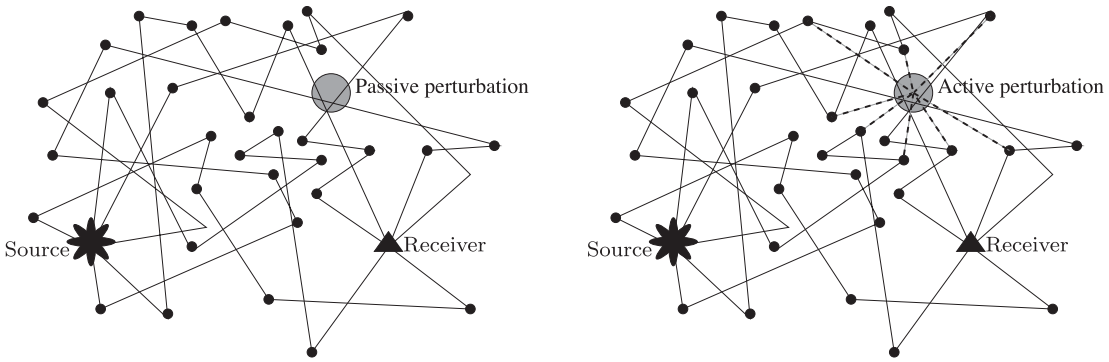

Figure 1. Passive (left) versus active (right) medium perturbations. The filled circles and solid lines represent distributed heterogeneities and multiple-scattering trajectories, respectively. Depending on its effect on the propagation paths, a medium perturbation (shaded area) may be qualified as passive or active. A passive perturbation (left) is assumed not to affect the propagation paths in the medium. An active perturbation (right) generates new propagation paths in the medium through an additional scattering event. These new trajectories are represented by thick dashed lines. Depending on the observable, a perturbation may be considered as passive, active, or both (see the text for details).

angular integral of G which we denote by $I(\mathbf{r}, t; \mathbf{r}_0, \mathbf{n}_0)$. It represents the total probability to be detected at $\mathbf{r}$ at time t. In the case of an isotropic source, we denote by $I(\mathbf{r}, t, \mathbf{n}; \mathbf{r}_0)$ the probability that a seismic phonon launched at $t = 0$ be detected in direction $\mathbf{n}$, at time t and position $\mathbf{r}$. This quantity may again be interpreted as a specific intensity in the framework of transport theory. Finally, we introduce $I(\mathbf{r}, t, ; \mathbf{r}_0)$, the probability that a seismic phonon which has been launched at $t = 0$ by the isotropic source is located at $\mathbf{r}$ at time t. The following relations hold:

$$I(\mathbf{r}, t, \mathbf{n}; \mathbf{r}_0) = \frac{1}{S^d} \int_{S^d} G(\mathbf{r}, t, \mathbf{n}; \mathbf{r}_0, \mathbf{n}_0) dn_0 \tag{1a}$$

$$I(\mathbf{r}, t; \mathbf{r}_0) = \int_{S^d} I(\mathbf{r}, t, \mathbf{n}; \mathbf{r}_0) dn \tag{1b}$$

$$I(\mathbf{r}_0, t, -\mathbf{n}_0; \mathbf{r}) = \frac{1}{S^d} I(\mathbf{r}, t; \mathbf{r}_0, \mathbf{n}_0) \tag{1c}$$

where S^d denotes the unit sphere in space dimension d, as well as its area in a slight abuse of notation. The factor $1/S^d$ in the RHS of eqs (1a) and (1c) is required to preserve the normalization of probabilities. Eq. (1c) is a basic reciprocity relation in transport theory (Case & Zweifel 1967). To facilitate the understanding of the derivations, Table 1 summarizes the various probability distributions introduced in eqs (1a)–(1c). Note again that all probabilities are normalized in the sense that integration over $\mathbf{r}$ (for omni-directional detection), or over $\mathbf{r}$ and $\mathbf{n}$ (for mono-directional detection) yields 1 at all times. It is also worth noting that the probability distributions appearing in Table 1 are Green's functions of the transport equation to be introduced in Section 3 (Green's function calculation). As such, their dimension is $[L]^{-d}$, where $[L]$ stands for length and d is the space dimension. This further justifies their interpretation as probability densities.

Let us now consider the following typical problem in coda-wave interferometry. A slight relative change of background velocity $\delta c/c$ occurs in a small volume $dV(\mathbf{r}')$ of the propagation medium between two data acquisitions. If the scatterers are away from resonance, such a change will not affect the propagation paths in the heterogeneous medium, but will manifest itself as a small lapse-time-dependent shift of waveforms (Snieder 2006). To predict the time-shift, we need to evaluate the typical time spent in $dV(\mathbf{r}')$ by seismic phonons propagating from source to receiver. This problem may be formulated probabilistically as follows. Consider an isotropic source of seismic phonons acting at $\mathbf{r}_0$ and $t = 0$. Let A denote the following event: a seismic phonon propagating in direction $\mathbf{n}'$ is detected at time t' in the volume $dV(\mathbf{r}')$. Let

Table 1. Pictorial explanation of the four probability distributions introduced in the text.

Source	Mono-directional	Mono-directional	Isotropic	Isotropic
Detection	Mono-directional	Omni-directional	Mono-directional	Omni-directional
Notation	$G(\mathbf{r}, t, \mathbf{n}; \mathbf{r}_0, \mathbf{n}_0)$	$I(\mathbf{r}, t; \mathbf{r}_0, \mathbf{n}_0)$	$I(\mathbf{r}, t, \mathbf{n}; \mathbf{r}_0)$	$I(\mathbf{r}, t; \mathbf{r}_0)$
				

B denote the event: a seismic phonon reaches the receiver $\mathbf{r}$ at time t (in any propagation direction). We want to evaluate the probability of A conditioned by B ($P(A|B)$). Application of Bayes formula yields:

$$P(A|B) = \frac{P(B|A)P(A)}{P(B)} = \frac{I(\mathbf{r}, t-t'; \mathbf{r}', \mathbf{n}')I(\mathbf{r}', t', \mathbf{n}'; \mathbf{r}_0)dV(\mathbf{r}')}{I(\mathbf{r}, t; \mathbf{r}_0)} \tag{2}$$

From eq. (2), we deduce the total time T_e spent by seismic phonons propagating in direction $\mathbf{n}'$ in the volume $dV(\mathbf{r}')$ as the integral over all possible times t'. This leads to a temporal convolution of specific intensities:

$$T_e(dV(\mathbf{r}'), \mathbf{n}', t; \mathbf{r}, \mathbf{r}_0) = dV(\mathbf{r}') \int_0^t \frac{I(\mathbf{r}, t-t'; \mathbf{r}', \mathbf{n}')I(\mathbf{r}', t', \mathbf{n}'; \mathbf{r}_0)dt'}{I(\mathbf{r}, t; \mathbf{r}_0)} \tag{3}$$

At this point, our formalism still keeps track of the propagation direction $\mathbf{n}'$ of the phonons, which may be useful when the velocity perturbation is *anisotropic*. In the isotropic case, we may integrate over all possible intermediate propagation directions $\mathbf{n}'$ to obtain the traveltime shift induced by a local, weak change of velocity:

$$\begin{aligned}\delta t &= -\frac{\delta c}{c}(\mathbf{r}') \int_{S^d} T_e(dV(\mathbf{r}'), \mathbf{n}', t; \mathbf{r}, \mathbf{r}_0)dn' \\ &= -\frac{\delta c}{c}(\mathbf{r}')K_{tt}(\mathbf{r}', t; \mathbf{r}, \mathbf{r}_0)dV(\mathbf{r}')\end{aligned} \tag{4}$$

Eq. (4) introduces the traveltime or passive sensitivity kernel K_{tt}:

$$K_{tt}(\mathbf{r}', t; \mathbf{r}, \mathbf{r}_0) = S^d \int_0^t \int_{S^d} \frac{I(\mathbf{r}', t-t', -\mathbf{n}'; \mathbf{r})I(\mathbf{r}', t', \mathbf{n}'; \mathbf{r}_0)dt'dn'}{I(\mathbf{r}, t; \mathbf{r}_0)} \tag{5}$$

where the reciprocity theorem (1c) has been used in the final expression. Note that the intensity I has dimension $[L]^{-d}$ (Paasschens 1997) so that the kernel has dimension $[t][L]^{-d}$. The same sensitivity kernel has already surfaced in the seismological literature in the context of mapping the spatial distribution of absorption in the Earth using coda waves (Mayor *et al.* 2014). Note that the theory should also be valid when the medium is absorbing, although the normalization of probability breaks down in this case. In the case of uniform absorption, the validity of eq. (5) is obvious, as the extra exponential decay terms entailed by dissipation cancel out of the expression. Physically, the kernel K_{tt} allows one to keep track of the phonons that propagate from $\mathbf{r}_0$ to $\mathbf{r}$ in time t. An observer who could visualize all seismic phonon trajectories in the medium would be able to evaluate K_{tt} by measuring the time spent inside the volume dV by each phonon reaching the receiver, as a function of the lapse time t (see Fig. 1). In this sense, the kernel (5) may indeed be deemed 'passive'. The kernel (5) differs from the one derived by Pacheco & Snieder (2005) simply because their approach relies on a diffusion approximation, which assumes that the anisotropy of the energy flux is negligible. When this condition applies, the specific intensity may be replaced by its angular average and the result of Pacheco & Snieder (2005) is recovered. Note however that the diffusion approximation always breaks down in the vicinity of the source/receiver.

We now consider a perturbation of the medium, such as damaging, magma injection or fracturing which locally modifies the scattering properties. Such a medium change will entail the creation of new propagation paths between source and receiver which in turn result in a distortion of waveforms in the coda. The distortion effect may be quantified by a decorrelation coefficient defined as (Planès *et al.* 2014):

$$dc(t) = 1 - \frac{\langle u_1(t)u_2(t)\rangle}{\sqrt{I_1(t)I_2(t)}}, \tag{6}$$

where $u_{1,(2)}$ denotes the wavefield acquired at date 1 (respectively 2), $I_{1,(2)}(t) = \langle u_{1,(2)}(t)^2\rangle$ and the brackets represent an ensemble average. In practice, averaging is performed over a short time window in the coda. Strictly speaking, I_1 (or I_2) is not an intensity. However, if we think of $u_1(t)$ as the velocity of ground motions, then multiplication of $\langle u_1(t)^2\rangle$ by a factor $\rho c/2$, with ρ the mass density and c the wave speed, does convert I_1 into an intensity. Clearly, the decorrelation coefficient increases from 0 to 1 as the effect of distortion becomes more and more pronounced. If the changes in the medium are not too large, the intensities at date 1 and 2 will differ only slightly, which allows us to introduce a number ϵ such that $I_2 = I_1(1+\epsilon)$. For small ϵ, the difference between the geometric and arithmetic average is of order ϵ^2 only, which allows us to rewrite the decorrelation coefficient as:

$$dc(t) \approx 1 - \frac{2\langle u_1(t)u_2(t)\rangle}{I_1(t)+I_2(t)} \approx \frac{\langle (u_2(t)-u_1(t))^2\rangle}{I_1(t)+I_2(t)} \approx \frac{\langle (u_2(t)-u_1(t))^2\rangle}{2I_1(t)}(1-\epsilon/2) \tag{7}$$

In the last equality of eq. (7), the second term inside the parentheses is a small intensity correction which will be neglected. In the denominator, I_1 may be interpreted—up to a pre-factor $\rho c/2$—as the intensity at time t in the coda before the change, an approximation of which is supposed to be known. Similarly, the numerator may be interpreted as an extra intensity scattered by the local change of mechanical properties, which will be modeled by the addition of scatterers in the medium. We denote by σ and $f(\mathbf{n}, \mathbf{n}')$ their scattering cross-section and normalized differential cross-section, respectively. In the radiative transfer literature, $f(\mathbf{n}, \mathbf{n}')$ is also called 'phase function' and gives the probability that a phonon propagating in direction $\mathbf{n}'$ be deflected into direction $\mathbf{n}$. For an isotropic point source, the amount of energy propagating in direction $\mathbf{n}'$ through a small surface $dS(\mathbf{r}')$ with normal $\mathbf{n}'$ in the time interval $[t', t'+dt']$ is given by $F_0 I(\mathbf{r}, t', \mathbf{n}'; \mathbf{r}_0)dS(\mathbf{r}')dt'$. Recalling that the Green's function $I(\mathbf{r}, t', \mathbf{n}'; \mathbf{r}_0)$ has dimension $[L]^{-d}$, F_0 serves as a source term which ensures that the product $F_0 \times I$ has the correct units for intensity (i.e. $\mathrm{Jm}^{d-1}\mathrm{s}^{-1}$, with d the space dimension). Let us assume that the small volume $dV(\mathbf{r}') = dS(\mathbf{r}')cdt'$ (c is the wave speed)

contains $N = d(\mathbf{r}')dV(\mathbf{r}')$ new scatterers with number density $d(\mathbf{r}')$. A basic principle in transport theory stipulates that the total amount of intensity scattered off the incoming phonon beam is proportional to the ratio between the total scattering cross-section $N\sigma$ and the surface element $dS(\mathbf{r}')$ (e.g. Kourganoff 1969, p.36). Furthermore, taking into account that only the fraction $f(\mathbf{n}, \mathbf{n}')$ is deflected from direction $\mathbf{n}'$ to direction $\mathbf{n}$, we obtain the following expression for the extra intensity emitted at time t' and position $\mathbf{r}'$ into direction $\mathbf{n}$:

$$\delta I = cdt'\sigma d(\mathbf{r}')f(\mathbf{n}, \mathbf{n}')I(\mathbf{r}', t', \mathbf{n}'; \mathbf{r}_0)F_0 \tag{8}$$

The next step of our derivation consists in propagating the intensity δI from $\mathbf{r}'$ to the detector $\mathbf{r}$. This may be achieved with the aid of the Green's function depicted in the second column of Table 1. The extra scattered intensity produced in the volume $dV(\mathbf{r}')$ between t' and $t' + dt'$ and recorded at $\mathbf{r}$ at time t is therefore given by:

$$\delta I_{\rm sc} = d(\mathbf{r}')dV(\mathbf{r}')cdt'\sigma I(\mathbf{r}, t - t'; \mathbf{r}', \mathbf{n})f(\mathbf{n}, \mathbf{n}')I(\mathbf{r}', t', \mathbf{n}'; \mathbf{r}_0)F_0 \tag{9}$$

It may be readily verified that $\delta I_{\rm sc}$ has the units of an intensity as it should. At this stage, we still keep track of all the details of the scattering process, that is, we follow exactly those phonons which are incident at $\mathbf{r}'$ in direction $\mathbf{n}'$ and are scattered into direction $\mathbf{n}$. Such a formulation is necessary to retrieve the full angular dependence of the scattering cross-section from the data. The overall decorrelation produced by the extra scatterers may now be evaluated by reporting eq. (9) into eq. (7) and integrating over all propagation directions and over time:

$$\mathrm{dc}(t) = \frac{d(\mathbf{r}')dV(\mathbf{r}')c\sigma S^d}{2}\int_0^t\int_{S^d}\int_{S^d}\frac{I(\mathbf{r}', t - t', -\mathbf{n}; \mathbf{r})f(\mathbf{n}, \mathbf{n}')I(\mathbf{r}', t', \mathbf{n}'; \mathbf{r}_0)dt'dn'dn}{I(\mathbf{r}, t; \mathbf{r}_0)} \tag{10}$$

Note that we have made use of the reciprocity relation (1c), and that upon normalization by I_1 the source term F_0 has canceled out. The result (10) has been established for a change localized in a small volume $dV(\mathbf{r}')$. In the case of an extended change, the total decorrelation may be obtained by integration over $\mathbf{r}'$. We may further simplify the analysis by assuming that the new scatterers are small enough with respect to the wavelength to consider that their scattering pattern is isotropic ($f(\mathbf{n}', \mathbf{n}) = 1/S^d$). The angular integrals may be performed thanks to eq. (1b) which yields:

$$\mathrm{dc}(t) = \frac{d(\mathbf{r}')dV(\mathbf{r}')c\sigma}{2}K_{\rm dc}(\mathbf{r}', t; \mathbf{r}, \mathbf{r}_0), \tag{11}$$

where we have introduced the following decorrelation or active sensitivity kernel:

$$K_{\rm dc}(\mathbf{r}', t; \mathbf{r}, \mathbf{r}_0) = \int_0^t \frac{I(\mathbf{r}', t - t'; \mathbf{r})I(\mathbf{r}, t'; \mathbf{r}_0)dt'}{I(\mathbf{r}, t; \mathbf{r}_0)} \tag{12}$$

This formula was previously obtained by Planès *et al.* (2014) based on a diagrammatic approach in the diffusion regime. Our derivation provides support for the validity of this formula in the radiative transfer regime. Again, the result (12) is valid in the presence of uniform absorption too. The kernel $K_{\rm dc}$ takes into account the new propagation paths which have been created thanks to the addition of scatterers in the medium. In this sense, this kernel may be deemed 'active'. The chief difficulty in applying the sensitivity kernels (5) and (12) to coda-wave interferometry comes from the fact that the Green's function of the radiative transfer equation is hard to evaluate either analytically or numerically. In what follows, we take advantage of recent advances in spectral techniques (Panasyuk *et al.* 2006) to evaluate numerically the traveltime and decorrelation sensitivity kernels in 2-D anisotropically scattering media. The next section is devoted to a brief description of the spectral technique, and its validation against Monte Carlo simulations.

3 GREEN'S FUNCTION CALCULATION

In this section, we describe the method used to calculate the solution of the radiative transfer equation for a point-like, isotropic, impulsive source of intensity in a statistically homogeneous medium:

$$\frac{\partial I(\mathbf{r}, t, \mathbf{n})}{\partial t} + c\mathbf{n}\cdot\nabla I(\mathbf{r}, t, \mathbf{n}) + \left(\frac{1}{\tau_a} + \frac{1}{\tau_s}\right)I(\mathbf{r}, t, \mathbf{n}) = \frac{1}{\tau_s}\int_{2\pi} p(\mathbf{n}, \mathbf{n}')I(\mathbf{r}, t, \mathbf{n}')d\mathbf{n}' + \delta(\mathbf{r})\delta(t) \tag{13}$$

In eq. (13) c denotes the wave speed, $\tau_a = Q_i(\omega)/\omega$ is the absorption time and $\tau_s = Q_{\rm sc}(\omega)/\omega$ is the scattering mean-free time. Q_i and $Q_{\rm sc}$ are the usual frequency-dependent intrinsic and scattering quality factors, respectively. The normalized differential cross-section $p(\mathbf{n}, \mathbf{n}')$ describes the scattering anisotropy in the propagation medium. We have purposely employed a new notation to distinguish it from the scattering anisotropy of the medium change—denoted by $f(\mathbf{n}, \mathbf{n}')$ in Section 2— because the two quantities are *a priori* different. Note that to be fully consistent with the notations introduced in Table 1, we should have denoted the specific intensity by $I(\mathbf{r}, t, \mathbf{n}; \mathbf{0})$ ($\mathbf{0}$ is the zero vector). Since the medium is translationally invariant, the use of two spatial variables becomes redundant and we have simplified the notations accordingly.

The symmetry of the problem imposes that the specific intensity depend solely on the time t, the source–receiver distance r and the angle ϕ_r between the propagation direction $\hat{\mathbf{n}}$ and the position vector $\mathbf{r} = r\hat{\mathbf{r}} = (r\cos\varphi_{\mathbf{r}}, r\sin\varphi_{\mathbf{r}})$ (see Fig. 2 for an illustration of the notations). In this geometry, the radiative transfer equation may be rewritten as:

$$\left(\frac{\partial}{\partial t} + c\cos(\phi_r)\frac{\partial}{\partial r} - c\sin(\phi_r)\frac{\partial}{r\partial\phi_r}\right)\mathcal{I}(r, t, \phi_r) + \left(\frac{1}{\tau_a} + \frac{1}{\tau_s}\right)\mathcal{I}(r, t, \phi_r) = \frac{1}{\tau_s}\int_0^{2\pi} p(\phi_r, \phi_r')\mathcal{I}(r, t, \phi_r')d\phi_r' + \frac{\delta(r)}{2\pi r}\delta(t), \tag{14}$$

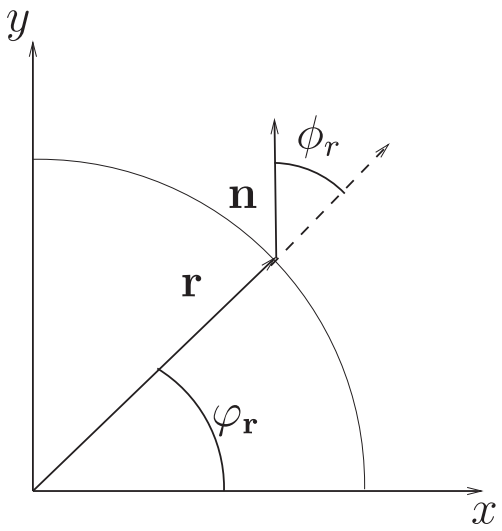

Figure 2. Definition of the geometrical variables used in the text.

where $I(\mathbf{r}, t, \mathbf{n}) = \mathcal{I}(|\mathbf{r}|, t, \phi_r)$ with $\mathbf{n} = (\cos(\varphi_{\mathbf{r}} + \phi_r), \sin(\varphi_{\mathbf{r}} + \phi_r))$. In the rest of the paper, we will use the notation I to represent the specific intensity, independent of the set of variables employed. The meaning should be clear from the context. Following Liemert & Kienle (2011), we expand the specific intensity in a Fourier–Bessel series:

$$I(r, t, \phi_r) = \sum_{m=0}^{m=\infty} a_m \cos(m\phi_r) \int_0^{+\infty} J_m(kr) k dk \int_{-\infty}^{+\infty} \tilde{I}_m(k, \Omega) e^{-i\Omega t} d\Omega, \tag{15}$$

where J_m denotes the regular Bessel function of order m and the constants a_m take the following values: $a_0 = 1/(4\pi)$, $a_m = 1/(2\pi)$ for $m > 0$. Note that we have carefully distinguished between the central frequency of the waves ω and the modulation frequency Ω, the latter being the Fourier conjugate variable of the lapse time t. The forward transform is given by:

$$\tilde{I}_m(k, \Omega) = \frac{1}{\pi} \int_0^{2\pi} \cos(m\phi_r) d\phi_r \int_{-\infty}^{+\infty} e^{i\Omega t} dt \int_0^{+\infty} J_m(kr) I(r, t, \phi_r) r dr \tag{16}$$

Reporting expansion (15) into the radiative transfer eq. (14), one obtains the following tridiagonal system for the unknowns $\tilde{I}_m(k, \Omega)$:

$$(-i\Omega + 1/\tau_a + 1/\tau_s(1 - p_m))\tilde{I}_m(k, \Omega) + \frac{ck}{2}(\tilde{I}_{m+1} - \tilde{I}_{m-1})(k, \Omega) = \tilde{S}_m(k, \Omega), \tag{17}$$

with $\tilde{I}_{-1} = -\tilde{I}_1$. In eq. (17), $\tilde{S}$ denotes the source of intensity and the p_m are the Fourier coefficients of the phase function p:

$$p(\phi_r, \phi_r') = p(\cos(\phi_r - \phi_r')) = \frac{1}{\pi}\left[\frac{1}{2} + \sum_{m>0} p_m \cos(m(\phi_r - \phi_r'))\right], \tag{18}$$

where $p_0 = 1$ because the phase function is normalized. Note that there is a slight abuse of notation in eq. (18): the same symbol p is employed to denote the phase function expressed either in terms of the incoming and outgoing scattering angle, or in terms of the cosine of the scattering angle. In the same vein, we will also denote by $p(\mathbf{n}, \mathbf{n}')$ the probability of scattering from direction $\mathbf{n}'$ to direction $\mathbf{n}$. Sato (1994) has developed an alternative Fourier–Bessel representation of the Green's function of the radiative transfer equation. His starting point is the integral form of the transfer equation, so that the system of equations to be solved differs from (14). It will be interesting to further compare the integral and integro-differential formulations in the future.

In the numerical applications, we employ the Henyey–Greenstein phase function which is defined by $p_m = g^m$, where g is the mean cosine of the scattering angle. In this case, summation of the series (18) yields:

$$p(\phi_r, \phi_r') = \frac{1 - g^2}{2\pi(1 + g^2 - 2g\cos(\phi_r - \phi_r'))}. \tag{19}$$

Provided the following identification is made: $g = (1 + 2k^2a^2 - \sqrt{1 + 4k^2a^2})/2k^2a^2$, the Henyey–Greenstein model can be considered as an end-member of the general Von-Karman phase function of the form:

$$p(\phi_r, \phi_r') = \frac{N(ka, \kappa)}{(1 + 2k^2a^2(1 - \cos(\phi_r - \phi_r'))^{\kappa+1}} \tag{20}$$

in the limit $\kappa \to 0$ (see Sato *et al.* 2012, p. 24). In eq. (20), $N(ka, \kappa)$ denotes a normalization factor which guarantees that the integral of p over $\phi_r \in [0, 2\pi]$ equals 1.

At very low frequency, inhomogeneities are small compared to the wavelength and scattering is usually isotropic (or non-preferential), which corresponds to the case $g = 0$. As the wavelength decreases (or as the frequency increases), waves become sensitive to the details of

the inhomogeneities and a peak of scattering usually develops around the forward direction (see e.g. Sato *et al.* 2012, p. 132). As a result, g increases with frequency (but remains always bounded below 1). This prediction is in agreement with recent observations and models of crustal coda waves by Calvet *et al.* (2013). In seismology, the Henyey–Greenstein phase function has been introduced by Margerin & Nolet (2003) to model wave scattering in the lower mantle in connection with the spatiotemporal distribution of *PKP* precursors.

Liemert & Kienle (2011) solve a system equivalent to eq. (17) for the total intensity including the coherent contribution. In this work, following Sato (1994) we subtract the coherent and single-scattering terms from the total intensity. In this way, the convergence of the series expansion for the multiple-scattering intensity is substantially improved, and exact analytical expressions can be employed for the singular terms. We recall that the coherent wave carries the fraction of intensity which has not been scattered at all. This wave decays exponentially with the distance to the source. The single-scattering term corresponds to waves which have changed propagation direction only once since their departure from the source. Together with higher order scattering terms, they form the diffuse intensity. The calculation of the coherent and single-scattering terms in the space–time and transformed domains is detailed in the next paragraph.

As previously noted, the coherent term $I^c(r,\, t,\, \phi_r)$ corresponds to the part of the intensity which propagates from source to receiver without undergoing any scattering event. This term satisfies the following equation:

$$\left(\frac{\partial}{\partial t} + c\cos(\phi_r)\frac{\partial}{\partial r} - c\sin(\phi_r)\frac{\partial}{r\partial\phi_r}\right)I^c(r,t,\phi_r) + \left(\frac{1}{\tau_a}+\frac{1}{\tau_s}\right)I^c(r,t,\phi_r) = \frac{\delta(r)\delta(t)}{2\pi r} \tag{21}$$

and can be expressed analytically as (Paasschens 1997):

$$I^c(r,t,\phi_r) = \frac{\delta(r-ct)\delta(\phi_r)}{r}e^{-t/\tau_e}H(t), \tag{22}$$

where we have introduced the inverse extinction time: $1/\tau_e = 1/\tau_a + 1/\tau_s$, and where H denotes the Heaviside distribution. Eq. (22) confirms the exponential decay of the coherent wave. In the Fourier–Bessel domain, the coherent term may be expressed as (Gradshteyn & Ryzhik 2007, p. 694):

$$\tilde{I}^c_m(k,\Omega) = \frac{(\sqrt{k^2+\alpha^2}-\alpha)^m}{\pi c k^m\sqrt{k^2+\alpha^2}}, \tag{23}$$

where $\alpha = (1/\tau_a + 1/\tau_s - i\Omega)/c$.

The single-scattering term corresponds to the part of the intensity which has been scattered only once on its path from source to station. This term is the solution of the following equation:

$$\left(\frac{\partial}{\partial t} + c\cos(\phi_r)\frac{\partial}{\partial r} - c\sin(\phi_r)\frac{\partial}{r\partial\phi_r} + \frac{1}{\tau_e}\right)I^{sg}(r,t,\phi_r) = \frac{1}{\tau_s}\int_0^{2\pi} p(\phi_r,\phi_r')I^c(r,t,\phi_r')d\phi_r' = \frac{p(\cos\phi_r)e^{-t/\tau_e}\delta(r-ct)H(t)}{\tau_s r} \tag{24}$$

and can be expressed as:

$$I^{sg}(r,t,\phi_r) = \frac{p(\mathbf{n}\cdot\hat{\mathbf{r}}_s(t))e^{-t/\tau_e}H(ct-r)}{c\tau_s(ct-r\cos\phi_r)}, \tag{25}$$

where $\mathbf{r}_s(t)$ is the position vector of the scatterer which contributes to the intensity propagating in direction $\mathbf{n}$, at time t at the receiver. As usual, the hat ˆ indicates a unit vector. The cosine of the scattering angle can be expressed as:

$$\mathbf{n}\cdot\hat{\mathbf{r}}_s(t) = \frac{2r^2\sin^2\phi}{r^2-2ctr\cos\phi+c^2t^2} - 1. \tag{26}$$

Eq. (25) may be obtained by convolving the source term $S(\mathbf{r},t,\mathbf{n}) = p(\hat{\mathbf{n}},\hat{\mathbf{r}})H(t)e^{-t/\tau_e}\delta(r-ct)/r$ in the right-hand side of eq. (24) with the coherent Green's function $G^c(\mathbf{r},t,\mathbf{n};\mathbf{r}_0,\mathbf{n}_0) = \delta(\mathbf{r}-\mathbf{r}_0-ct\mathbf{n}_0)\delta(\mathbf{n}-\mathbf{n}_0)e^{-t/\tau_e}H(t)$. The latter is the solution of eq. (24) for a directional and point-like unit source (see first column of Table 1). To find the expression of the single-scattering term in the Fourier–Bessel domain, it is convenient to write it again as a convolution integral in the frequency domain:

$$I^{sg}(\mathbf{r},\Omega,\mathbf{n}) = \frac{1}{c^2\tau_s}\int_{\mathbb{R}^2}\frac{e^{-\alpha(r_s+|\mathbf{r}-\mathbf{r}_s|)}}{r_s|\mathbf{r}-\mathbf{r}_s|}\delta\left(\frac{\mathbf{r}-\mathbf{r}_s}{|\mathbf{r}-\mathbf{r}_s|}-\mathbf{n}\right)p(\mathbf{n}\cdot\hat{\mathbf{r}}_s)d\mathbf{r}_s, \tag{27}$$

with $\alpha = (i\Omega + 1/\tau_e)/c$. The transform of the convolution product can now be found in a straightforward manner using the results of Baddour (2009):

$$\tilde{I}^{sg}_m(k,\Omega) = \frac{(\sqrt{k^2+\alpha^2}-\alpha)^m}{\pi c^2\tau_s k^m(k^2+\alpha^2)}\left(\sum_{0\le q\le m} p_q + \sum_{q>0}(-1)^q(p_q+p_{m+q})\frac{(\sqrt{k^2+\alpha^2}-\alpha)^{2q}}{k^{2q}}\right) \tag{28}$$

In the case of the Henyey–Greenstein phase function, the sums inside the parenthesis can be performed analytically which yields closed form expressions for the single-scattering intensity in the transformed domain. Using eqs (18) and (28), the source term for the multiple-scattering intensity can be expressed as:

$$\tilde{S}_m(k,\Omega) = \frac{p_m}{\tau_s}\tilde{I}^{sg}_m(k,\Omega) \tag{29}$$

The system of eq. (17) with the source term (29) can be solved using standard linear algebra libraries such as LAPACK. To transform the multiple-scattering solution $\tilde{I}_m^{hi}(k, \Omega)$ back to the (r, t, ϕ_r) domain, the continuous Hankel and Fourier transforms are replaced by their discrete versions. In practice, the intensity was evaluated at 384 points in the frequency domain with $\Delta f = 0.23/\pi$. This choice allows us to evaluate the specific intensity up to a lapse time $t = 12$ mean-free times in the coda, which should be sufficient for most applications. As a rule, the spatial domain considered in the simulation has a radius $R = c/\Delta f$, where Δf is the step size in the frequency domain. Regarding the discretization of the angular and spatial domains, we typically retain 124 terms of the Fourier cosine expansion and evaluate $\tilde{I}_m$ at 1500 (for $g = 1/2$) and 2500 (for $g = 9/10$) discrete wavenumbers, respectively. After application of a discrete Hankel transform of order m (Johnson 1987), and of a fast inverse Fourier transform (Frigo & Johnson 2005), the complete solution can be written as:

$$I(r, t, \phi_r) = I^c(r, t, \phi_r) + I^d(r, t, \phi_r) = I^c(r, t, \phi_r) + I^{sg}(r, t, \phi_r) + \frac{1}{2} I_0^{hi}(r, t) + \sum_{m>0} I_m^{hi}(r, t) \cos m\phi_r, \tag{30}$$

where the analytical expression (25) for the single-scattering term can be employed for accuracy. Note that the formulae given above correspond to a non-normalized point source which injects a total intensity of 2π in the medium. To suppress high-frequency noise, the numerical solution is convolved with a normalized Kaiser–Bessel window defined as (Butz 2006):

$$K(t) = \frac{\beta I_0(\beta\sqrt{1 - (2t/T)^2})}{T \sinh \beta}. \tag{31}$$

The numerical results have been obtained with a window width $T = 0.25$ and a parameter $\beta = 22$.

In Fig. 3, we compare the results of the spectral approach and Monte Carlo simulations of the transport process obtained with a scalar version of the code developed by Margerin *et al.* (2000). We calculate the diffuse intensity at three angles $\phi_r = \pi/4, \pi/8, \pi/180$ from the forward and backward directions, in a random medium described by a Henyey–Greenstein phase function with anisotropy parameter $g = 0.5$ or $g = 0.9$. Note that in the exact forward direction the specific intensity diverges, which is impractical for numerical comparisons (hence the choice $\phi_r = \pi/180$). The source–receiver distance varies from $r = 0.05l$ to $r = 4.05l$ ($l = c\tau_s$ is the scattering mean-free path) and the absorption time is taken as $\tau_a = 2\tau_s$. Note that the two numerical solutions have been convolved with the same source time function (31). Excellent agreement is found between the two approaches, including in the vicinity of the source ($r = 0.05l$) for both weak and strong scattering anisotropy. The calculations reveal that a strong peak of intensity develops in the forward direction as the anisotropy parameter g increases. This point is further illustrated in Fig. 4, where we show snapshots of the scattered intensity field at lapse times $t = 3\tau_s, 6\tau_s$ for increasing values of the scattering anisotropy ($g = 0, 1/2, 2/3, 4/5$). Increasing the scattering anisotropy tends to concentrate the scattered intensity near the coherent front, giving rise to a large ballistic peak, which persists up to the transport mean-free time $\tau^* \approx \tau_s/(1 - g)$ in the coda. We recall that the transport mean-free time can be interpreted as the typical time for a wave to loose memory of its initial propagation direction. In the case of isotropic scattering, the randomization of propagation directions is complete after one scattering event only ($\tau^* = \tau_s$). To the contrary, when scattering anisotropy is strong, it takes a large number of scattering events before the propagation direction has been randomized ($\tau^* \gg \tau_s$). Interestingly, the spatial distribution of energy is rather flat behind the ballistic peak which is reminiscent of the energy flux model of Frankel & Wennerberg (1987). In the next two sections, the impact of scattering anisotropy on the sensitivity of coda waves is studied numerically based on the spectral formulation of the radiative transfer equation in 2-D.

4 TRAVELTIME SENSITIVITY KERNELS

In this section, we evaluate numerically the sensitivity kernel (5) in a variety of configurations which are relevant in seismology. We focus on relatively short propagation times (typically less than 8 mean-free times) and distances (less than five mean-free paths). In this weakly scattering regime, it is crucial to decompose the specific intensity into a sum of coherent and diffuse parts (Planès *et al.* 2014). In particular, the coherent intensity which is absent in the diffusion approximation (strong scattering regime) contributes significantly to the energy transport between source and receiver. This results in four contributions to the total sensitivity function: coherent–coherent, diffuse–coherent (and coherent-diffuse) and diffuse–diffuse. In the absence of scattering (i.e. in a homogeneous medium), all the energy is transported by coherent waves and it is instructive to examine this simple situation first. Substituting the coherent intensity I^c into eq. (5) and integrating over all space directions $\mathbf{n}$, the traveltime sensitivity kernel can be put into the following form:

$$K_{tt}^{cc}(\mathbf{r}', t; \mathbf{r}, \mathbf{r}_0) = \int_0^t \delta\left(\mathbf{r}' - \mathbf{r}_0 - ct' \frac{\mathbf{r} - \mathbf{r}_0}{|\mathbf{r} - \mathbf{r}_0|}\right) dt', \tag{32}$$

which demonstrates that the sensitivity is fully concentrated on the ray path between source and receiver. While this result does not come as a surprise, it is reassuring to see that radiative transfer theory contains as a special case the well-known predictions of geometrical optics.

We now examine the general situation of a scattering and absorbing medium. The coherent–diffuse term may be expressed as:

$$\begin{aligned} K_{tt}^{cd}(\mathbf{r}', t; \mathbf{r}, \mathbf{r}_0) &= \frac{2\pi}{I(\mathbf{r}, t; \mathbf{r}_0)} \int_{\mathbb{R}} \int_{2\pi} I^d(\mathbf{r}' - \mathbf{r}, t - t', -\mathbf{n}) I^c(\mathbf{r}' - \mathbf{r}_0, t', \mathbf{n}) dt' d\mathbf{n} \\ &= \frac{e^{-|\mathbf{r}' - \mathbf{r}_0|/c\tau_e}}{c|\mathbf{r}' - \mathbf{r}_0| I(\mathbf{r}, t; \mathbf{r}_0)} I^d\left(\mathbf{r}' - \mathbf{r}, t - \frac{|\mathbf{r}' - \mathbf{r}_0|}{c}, \frac{\mathbf{r}_0 - \mathbf{r}'}{|\mathbf{r}' - \mathbf{r}_0|}\right) \end{aligned} \tag{33}$$

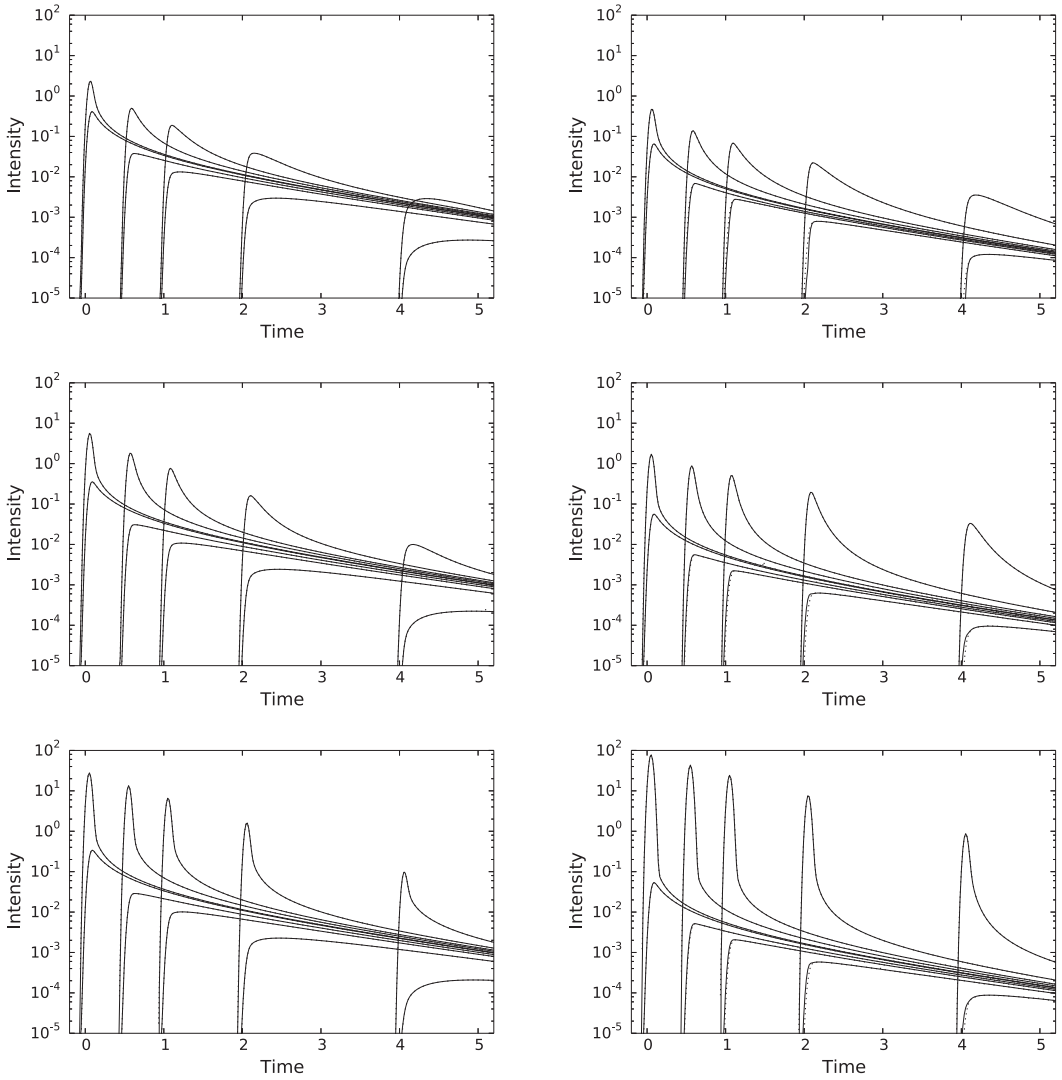

Figure 3. Diffuse intensity at $r = 0.05$, 0.55, 1.05, 2.05 and 4.05 mean-free paths from a point-like isotropic source. For each distance, the specific intensity is calculated in two opposite propagation directions. The angular deviation ϕ from the forward (or backward) propagation direction decreases from top to bottom: $\phi = \pi/4, \pi/8, \pi/180$. The random medium is described by a Henyey–Greenstein phase function with anisotropy parameter $g = 0.5$ (left) and $g = 0.9$ (right). The solid and dotted lines show the results of the Monte Carlo and spectral calculations, respectively. Good agreement is found between the two solutions.

The diffuse–coherent term is obtained by interchanging $\mathbf{r}$ and $\mathbf{r}_0$ in eq. (33). For completeness, we also give the expression of the diffuse–diffuse term:

$$K_{tt}^{dd}(\mathbf{r}', t; \mathbf{r}, \mathbf{r}_0) = \frac{2\pi}{I(\mathbf{r}, t; \mathbf{r}_0)} \int_{\mathbb{R}} \int_{2\pi} I^d(\mathbf{r}' - \mathbf{r}, t - t', -\mathbf{n}) I^d(\mathbf{r}' - \mathbf{r}_0, t', \mathbf{n}) dt' dn$$
$$= \frac{2\pi^2}{I(\mathbf{r}, t; \mathbf{r}_0)} \int_{\mathbb{R}} \left(\frac{I_0^d(|\mathbf{r}' - \mathbf{r}|, t - t') I_0^d(|\mathbf{r}' - \mathbf{r}_0|, t')}{2} + \sum_{m>0} (-1)^m I_m^d(|\mathbf{r}' - \mathbf{r}|, t - t') I_m^d(|\mathbf{r}' - \mathbf{r}_0|, t') \cos m(\varphi_{\mathbf{r}'-\mathbf{r}} - \varphi_{\mathbf{r}'-\mathbf{r}_0}) \right) dt', \tag{34}$$

where we have used the Fourier cosine expansion of the diffuse intensity to evaluate the angular integrals and $\varphi_{\mathbf{r}}$ denotes the angle between the vector $\mathbf{r}$ and the x-axis (see Fig. 2). Because the single-scattering intensity displays a singularity in the forward direction, this term should be evaluated—in all rigors—with the aid of the analytical result (25) and the spectral expansion (15) applied to the multiple-scattering intensity I^{hi} only. However, even for very anisotropic scattering ($g = 0.9$) and short distance from the source or receiver (typically of the order of $l/20$), the computational gain of the spectral expansion is so large, and the induced loss of accuracy so small, that it is almost always beneficial to use the cosine expansion of the single-scattering term. This is all the more true as the sensitivity is dominated by the coherent–diffuse(diffuse–coherent) term in the vicinity of the source(receiver), whose algebraic divergence is treated analytically. Pacheco & Snieder (2006) have developed a theory of traveltime perturbations of coda waves in the single-scattering regime and it seems worthwhile to briefly examine this case. To do so, we assume like Pacheco & Snieder (2006) that the transport is dominated by singly scattered waves ($I = I^{sg}$) and neglect higher order terms. We also assume isotropic scattering. The only terms that survive these assumptions are the coherent–diffuse

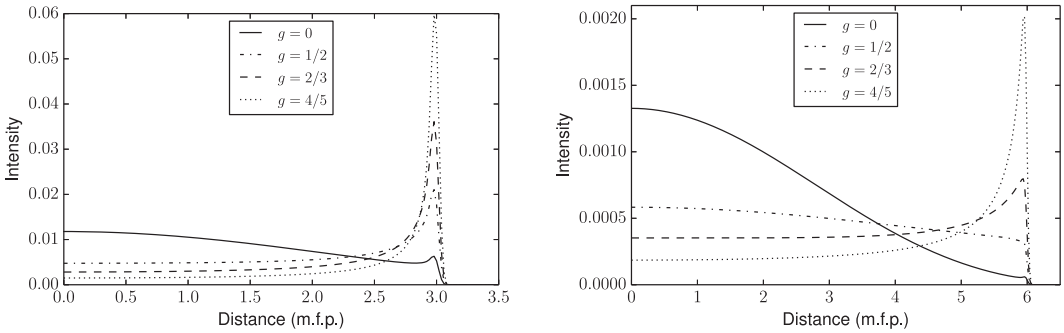

Figure 4. Snapshots of the spatial distribution of intensity in the coda at lapse time $t = 3\tau_s$ (left) and $t = 6\tau_s$ (right) for increasing levels of scattering anisotropy (see the legend). On the horizontal axis, the distance to the source is normalized by the scattering mean-free path. Note that the coherent intensity is independent of g and has not been plotted.

and diffuse–coherent terms. Inserting expressions (25) and (22)—after normalization of each term by a factor $1/2\pi$—into eq. (33) and integrating, we obtain:

$$K_{tt}^{sg} = \frac{1}{2\pi c^2 t}\left[\frac{\sqrt{c^2t^2-|\mathbf{r}-\mathbf{r}_0|^2}}{|\mathbf{r}'-\mathbf{r}_0|\left(1-\frac{(\mathbf{r}_0-\mathbf{r})\cdot(\mathbf{r}_0-\mathbf{r}')}{ct|\mathbf{r}_0-\mathbf{r}'|}\right)}+\frac{\sqrt{c^2t^2-|\mathbf{r}-\mathbf{r}_0|^2}}{|\mathbf{r}'-\mathbf{r}|\left(1-\frac{(\mathbf{r}'-\mathbf{r})\cdot(\mathbf{r}_0-\mathbf{r})}{ct|\mathbf{r}-\mathbf{r}'|}\right)}\right] \tag{35}$$

Using standard identities of analytic geometry, this equation may be shown to be equivalent to eq. (39) of Pacheco & Snieder (2006). Note however that these authors use slowness perturbations instead of velocity perturbations which causes slight notational differences. While radiative transfer successfully reproduces the single-scattering approximation as a limiting case, the theory incorporates effortlessly higher orders of scatterings, which constitutes a notable advantage. This point will be illustrated in detail in the rest of the paper.

For the numerical applications, we evaluate the sensitivity kernels on a fixed grid with horizontal and vertical spacings $0.04l$. The first row of gridpoints is located at $0.02l$ from the horizontal axis (X), in order to avoid the singularities at the source and receiver. Once the spectral expansion of the specific intensity has been obtained at each point of the grid, the calculation of the sensitivity kernels is immediate. Note that all the numerical results presented in this paper have been obtained after convolution of the exact specific intensity (including the coherent term) with the Kaiser–Bessel window (31). This procedure guarantees that the signal does not contain energy beyond the Nyquist frequency. In the case of isotropic scattering, we have reproduced the results of Mayor *et al.* (2014), which are based on the analytical solutions of Shang & Gao (1988) and Paasschens (1997), with excellent accuracy.

Fig. 5 illustrates the impact of anisotropic scattering on the traveltime sensitivity kernels (5). The reference isotropic case ($g = 0$) is shown on the left. The centre and right columns correspond to moderate ($g = 0.67$) and strong anisotropy ($g = 0.9$), respectively. The epicentral distance R and lapse time t in the coda increase from top to bottom as follows: $R = 0.48l$, $t = 2\tau_s$; $R = 0.96l$, $t = 4\tau_s$; $R = 1.92l$, $t = 6\tau_s$; $R = 3.84l$, $t = 8\tau_s$. In the Earth, the mean-free time (or mean-free path) varies over several orders of magnitude. Around 2 Hz for instance, the mean-free time can be as large as 500 s in the mantle (Margerin & Nolet 2003; Shearer & Earle 2004) and as small as 1 s in volcanic regions (Yamamoto & Sato 2010). Because the numerical value of the sensitivity depends strongly on a parameter which varies wildly in the Earth, we have chosen to normalize the kernels by the total spatial sensitivity, approximated by straightforward numerical summation. For the same reason, we have chosen to express all spatial and temporal measures in mean-free path and mean-free time units, respectively. This normalization procedure also facilitates the comparison of the sensitivity functions for different values of the anisotropy parameter g. In the case of crustal coda studies around a few hertz, the ratio between the epicentral distance (25–200 km) and the mean-free path (say 50 km) can typically vary between 0.5 and 4. Likewise, the ratio between the detection time (30–120 s) in the coda and the mean-free time (say 15 s) varies between 2 and 8. We therefore believe that the choice of parameters adopted in our study covers a number of practical situations. Of course, in real-case applications, the sensitivity should be calculated more precisely. Independent of the scattering anisotropy, the map of sensitivity is dominated by the coherent diffuse term, which diverges algebraically at the source and receiver. In the case of isotropic scattering, we observe that a zone of high sensitivity is located around the direct ray between source and station. This feature is much less pronounced in the case of moderate and strong anisotropic scattering. As scattering anisotropy increases, the diffusivity is enhanced and the scattered waves explore the propagation medium more rapidly. This effect may be quantified by considering the diffusivity of the multiply scattered waves. In the 2-D isotropic case, this parameter is given by $D_0 = c^2\tau_s/2$ and is related to the diffusivity D in the anisotropic case by $D = D_0/(1-g)$. For $g = 2/3$ or $g = 9/10$, we find that the diffusivity is enhanced by a factor 3 or 10, respectively. As a consequence, the sensitivity carried by the diffuse waves tends to be more uniformly distributed inside the causality (or single-scattering) ellipse. At sufficiently large epicentral distance and lapse time (bottom row, centre and right panels), one can clearly distinguish the short-range, high sensitivity of coherent waves superposed upon the slowly varying, weak sensitivity of diffuse waves. This shows that the coherent/incoherent decomposition of the intensity adopted in our approach is both mathematically convenient and physically sound.

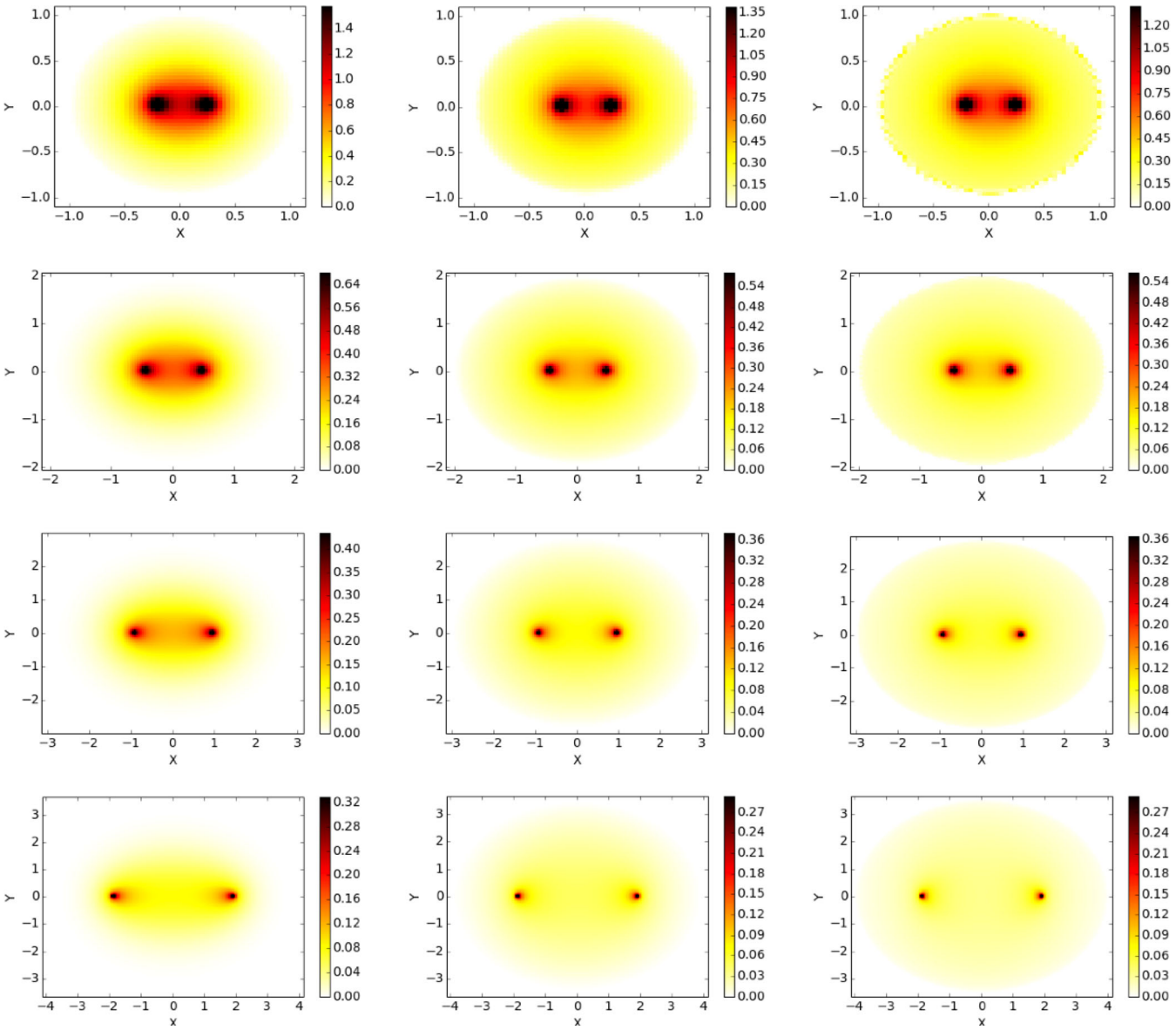

Figure 5. Traveltime sensitivity kernels of coda waves. The scattering anisotropy increases from left to right: $g = 0, 0.67, 0.9$. For each value of g, the kernels have been normalized by the total spatial sensitivity. The four rows correspond to the following epicentral distance and lapse time in the coda (from top to bottom): $R = 0.48l$, $t = 2\tau_s$; $R = 0.96l$, $t = 4\tau_s$; $R = 1.92l$, $t = 6\tau_s$; $R = 3.84l$, $t = 8\tau_s$. To facilitate the visualization, the colour scale has been saturated by clipping all values larger than half the maximum sensitivity.

5 DECORRELATION SENSITIVITY KERNEL

We pursue our exploration of sensitivity functions by considering the decorrelation kernel (12). We recall that decorrelation of coda waveforms is a manifestation of changes in the scattering properties of the medium. These changes may be represented by the addition of new scatterers with phase function $f(\mathbf{n}, \mathbf{n}')$. In the derivation that follows, we first consider an arbitrary f before specializing to the simple case of small objects which scatter waves isotropically ($f(\mathbf{n}, \mathbf{n}') = 1/2\pi$). Following again Planès *et al.* (2014), we express the total intensity as a sum of coherent and diffuse components, which in turn allows us to decompose the decorrelation sensitivity kernel into a sum of four contributions: coherent–coherent, coherent–diffuse (diffuse–coherent) and diffuse–diffuse. The coherent–coherent part can be written as:

$$K_{dc}^{cc}(\mathbf{r}', t; \mathbf{r}, \mathbf{r}_0) = \frac{2\pi}{I(\mathbf{r}, t; \mathbf{r}_0)} \int_0^t \int_{2\pi} \int_{2\pi} I^c(\mathbf{r}' - \mathbf{r}, t - t', -\mathbf{n}') f(\mathbf{n}', \mathbf{n}'') I^c(\mathbf{r}' - \mathbf{r}_0, t', \mathbf{n}'') dt' d\mathbf{n}' d\mathbf{n}'' \tag{36}$$

Substituting the expression of the coherent term (22) into eq. (36) and integrating yields:

$$K_{dc}^{cc}(\mathbf{r}', t; \mathbf{r}, \mathbf{r}_0) = \frac{e^{-(|\mathbf{r}'-\mathbf{r}|+|\mathbf{r}'-\mathbf{r}_0|)/c\tau_e}}{2\pi c|\mathbf{r}' - \mathbf{r}||\mathbf{r}' - \mathbf{r}_0| I(\mathbf{r}, t; \mathbf{r}_0)} f\left(\frac{\mathbf{r} - \mathbf{r}'}{|\mathbf{r} - \mathbf{r}'|}, \frac{\mathbf{r}' - \mathbf{r}_0}{|\mathbf{r}' - \mathbf{r}_0|}\right) \delta(|\mathbf{r}' - \mathbf{r}| + |\mathbf{r}' - \mathbf{r}_0| - ct), \tag{37}$$

which reduces to:

$$K_{dc}^{cc}(\mathbf{r}', t; \mathbf{r}, \mathbf{r}_0) = \frac{e^{-(|\mathbf{r}'-\mathbf{r}|+|\mathbf{r}'-\mathbf{r}_0|)/c\tau_e}}{(2\pi)^2 c|\mathbf{r}'-\mathbf{r}||\mathbf{r}'-\mathbf{r}_0| I(\mathbf{r}, t; \mathbf{r}_0)} \delta(|\mathbf{r}'-\mathbf{r}| + |\mathbf{r}'-\mathbf{r}_0| - ct) \tag{38}$$

in the case of an isotropically scattering perturbation, in agreement with Mayor *et al.* (2014). The sensitivity of the coherent-coherent term decays exponentially with the distance to the source and is fully concentrated on the single-scattering ellipse. Comparison with the coherent–coherent term of the traveltime sensitivity kernel (32) illustrates the importance of distinguishing between active and passive medium perturbations. The coherent–diffuse term can be expressed as:

$$\begin{aligned} K_{dc}^{cd}(\mathbf{r}', t; \mathbf{r}, \mathbf{r}_0) &= \frac{2\pi}{I(\mathbf{r}, t; \mathbf{r}_0)} \int_0^t \int_{2\pi} \int_{2\pi} I^d(\mathbf{r}'-\mathbf{r}, t-t', -\mathbf{n}') f(\mathbf{n}', \mathbf{n}'') I^c(\mathbf{r}'-\mathbf{r}_0, t', \mathbf{n}'') dt' d\mathbf{n}' d\mathbf{n}'' \\ &= \frac{e^{-|\mathbf{r}'-\mathbf{r}_0|/c\tau_e}}{c|\mathbf{r}'-\mathbf{r}_0| I(\mathbf{r}, t; \mathbf{r}_0)} \int_{2\pi} f\left(\mathbf{n}, \frac{\mathbf{r}'-\mathbf{r}_0}{|\mathbf{r}'-\mathbf{r}_0|}\right) I^d\left(\mathbf{r}'-\mathbf{r}, t - \frac{|\mathbf{r}_0-\mathbf{r}'|}{c}, -\mathbf{n}\right) d\mathbf{n} \\ &= \frac{e^{-|\mathbf{r}'-\mathbf{r}_0|/c\tau_e}}{c|\mathbf{r}'-\mathbf{r}_0| I(\mathbf{r}, t; \mathbf{r}_0)} \times \left[\frac{1}{2} I_0^d\left(|\mathbf{r}'-\mathbf{r}|, t - \frac{|\mathbf{r}_0-\mathbf{r}'|}{c}\right) + \sum_{m>0} (-1)^m f_m I_m^d\left(|\mathbf{r}'-\mathbf{r}|, t - \frac{|\mathbf{r}_0-\mathbf{r}'|}{c}\right) \cos m(\varphi_{\mathbf{r}'-\mathbf{r}} - \varphi_{\mathbf{r}'-\mathbf{r}_0})\right], \end{aligned} \tag{39}$$

which reduces to:

$$K_{dc}^{cd}(\mathbf{r}', t; \mathbf{r}, \mathbf{r}_0) = \frac{e^{-|\mathbf{r}'-\mathbf{r}_0|/c\tau_e}}{2c|\mathbf{r}'-\mathbf{r}_0| I(\mathbf{r}, t; \mathbf{r}_0)} I_0^d\left(|\mathbf{r}'-\mathbf{r}|, t - \frac{|\mathbf{r}_0-\mathbf{r}'|}{c}\right) \tag{40}$$

in the case of an isotropic perturbation. In eq. (39), the f_m are the Fourier coefficients of the phase function f of the medium change, akin to the p_m introduced in eq. (18). The diffuse–coherent term can be deduced from eqs (39) and (40) by interchanging $\mathbf{r}$ and $\mathbf{r}_0$. The diffuse–diffuse decorrelation kernel can likewise be expressed as:

$$\begin{aligned} K_{dc}^{dd}(\mathbf{r}', t; \mathbf{r}, \mathbf{r}_0) &= \frac{2\pi}{I(\mathbf{r}, t; \mathbf{r}_0)} \int_0^t \int_{2\pi} \int_{2\pi} I^d(\mathbf{r}'-\mathbf{r}, t-t', -\mathbf{n}') f(\mathbf{n}', \mathbf{n}'') I^d(\mathbf{r}'-\mathbf{r}_0, t', \mathbf{n}'') dt' d\mathbf{n}' d\mathbf{n}'' \\ &= \frac{2\pi^2}{I(\mathbf{r}, t; \mathbf{r}_0)} \int_0^t \left[\frac{1}{2} I_0^d(|\mathbf{r}'-\mathbf{r}|, t-t') I_0^d(|\mathbf{r}'-\mathbf{r}_0|, t') + \sum_{m>0} (-1)^m f_m I_m^d(|\mathbf{r}'-\mathbf{r}|, t-t') I_m^d(|\mathbf{r}'-\mathbf{r}_0|, t') \cos m(\varphi_{\mathbf{r}'-\mathbf{r}} - \varphi_{\mathbf{r}'-\mathbf{r}_0})\right] dt' \end{aligned} \tag{41}$$

which reduces to:

$$K_{dc}^{dd}(\mathbf{r}', t; \mathbf{r}, \mathbf{r}_0) = \frac{\pi^2}{I(\mathbf{r}, t; \mathbf{r}_0)} \int_0^t I_0^d(|\mathbf{r}'-\mathbf{r}|, t-t') I_0^d(|\mathbf{r}'-\mathbf{r}_0|, t') dt' \tag{42}$$

in the simple case of an isotropically scattering perturbation.

The impact of anisotropic scattering on the coda-wave decorrelation kernel is illustrated in Fig. 6, where we show sensitivity maps for increasing values of the mean cosine of the scattering angle: $g = 0$ (isotropic case, left), $g = 2/3$ (moderate anisotropy, centre) and $g = 9/10$ (strong anisotropy, right). The grid employed to discretize the sensitivity kernels, as well as the pairs (epicentral distance, lapse time) are the same as in Fig. 5 (from top to bottom: $R = 0.48l$, $t = 2\tau_s$; $R = 0.96l$, $t = 4\tau_s$; $R = 1.92l$, $t = 6\tau_s$; $R = 3.84l$, $t = 8\tau_s$). Three singularities show up very clearly at the source, the receiver and on the single-scattering ellipse in this figure, but their relative weights are strongly influenced by the details of the scattering. At fixed lapse time, we found that scattering anisotropy tends to concentrate the energy behind the coherent wave (see Fig. 4), which in turn strongly accentuates the sensitivity in the vicinity of the single-scattering ellipse. To confirm this interpretation, we note that the ballistic peak persists up to a lapse time $t \approx \tau^*$, which roughly corresponds to the time at which the causality ellipse starts to lose visibility in Fig. 6 (centre). In the case of the traveltime kernel K_{tt}, such a zone of high sensitivity was not visible (see Fig. 5). The different behaviours may be explained by an examination of eqs (5) and (12). In the former equation, we remark that the integrand is the product of a forward and a backward specific intensity. Keeping in mind that in the vicinity of the causality ellipse the intensity is strongly peaked in the forward direction, one easily deduces that the integrand in eq. (5) must be much smaller than the one in eq. (12), where a product of average intensities appears. Hence, the dissimilarity between Figs 5 and 6 follows.

Marked differences between the isotropic/anisotropic sensitivity maps persist at relatively long lapse time in the coda. In particular, while the sensitivity is concentrated around the direct ray path in the isotropic case, anisotropic scattering tends to uniformly increase the sensitivity in the bulk of the medium. This effect, which was also apparent in Fig. 5, is again related to the fact that diffusion is enhanced by scattering anisotropy, so that the multiply scattered waves fill the propagation volume all the more rapidly as g increases. This feature is again clearly visible on the snapshots shown in Fig. 4. These results clearly suggest that an estimation of scattering anisotropy is necessary to correctly map mechanical changes in the Earth using coda waves. In the case of volcanoes, seismological observations tend to favour an isotropic scattering model, but in the case of the crust the situation may be more complex and requires further analysis.

6 INTENSITY SENSITIVITY KERNELS

As a final illustration of our approach, we consider in this section the generalization of the intensity sensitivity kernels introduced by Mayor *et al.* (2014) to the case of isotropic scattering perturbations embedded in an otherwise anisotropically scattering medium. In this case,

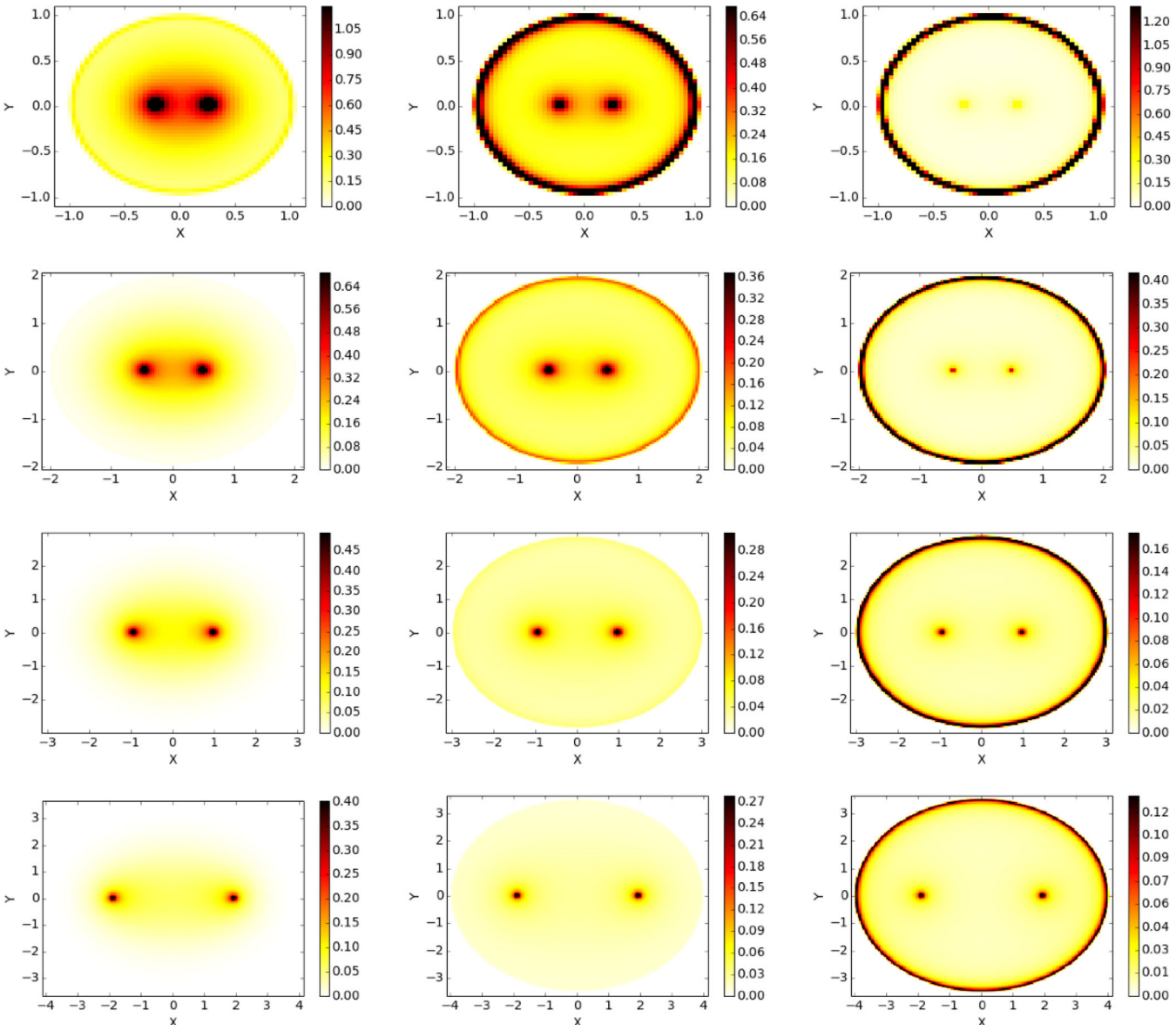

Figure 6. Decorrelation sensitivity kernels of coda waves. The scattering anisotropy increases from left to right: $g = 0$, 0.67, 0.9. For each value of g, the kernels have been normalized by the total spatial sensitivity. The four rows correspond to the following epicentral distance and lapse time in the coda (from top to bottom): $R = 0.48l$, $t = 2\tau_s$; $R = 0.96l$, $t = 4\tau_s$; $R = 1.92l$, $t = 6\tau_s$; $R = 3.84l$, $t = 8\tau_s$. To facilitate the visualization, the colour scale has been saturated by clipping all values larger than half the maximum sensitivity.

the focus is on the mapping of spatial variations of scattering properties from the spatiotemporal distribution of coda waves. To this end, following the classical tomographic approach, one imagines a reference medium upon which lateral perturbations of scattering properties are superposed. The objective is to relate deviations of the observed intensity from the one predicted in the reference medium to the lateral variations of scattering properties quantified by:

$$\delta Q_{\rm sc}^{-1}(\mathbf{r}) = Q_{\rm sc}^{-1}(\mathbf{r}) - Q_0^{-1}. \tag{43}$$

In eq. (43), Q_0^{-1} and $Q_{\rm sc}^{-1}(\mathbf{r})$ represent the scattering attenuation in the reference model and in the true Earth, respectively. Our assumption of isotropic scattering for the perturbation implies that the spatial variations of scattering attenuation are caused by geological features which are small compared to the wavelength. This assumption is by no means necessary but simplifies the analysis and does not seem too unreasonable.

Physically, a (say positive) perturbation of scattering properties located in a small volume $dV(\mathbf{r}')$ has two effects on the propagating intensity. First, the excess scattering removes a part of the energy from the waves that propagate through. To calculate the fraction of intensity lost in the process, it suffices to monitor all the seismic phonons that cross the volume $dV(\mathbf{r}')$, which is precisely what the passive kernel K_{tt} allows us to do. Second, the addition of scatterers to the medium gives rise to new propagation paths which in turn increase the probability for seismic phonons to reach the receiver. The fraction of intensity gained in the process can be directly evaluated with the aid of the active

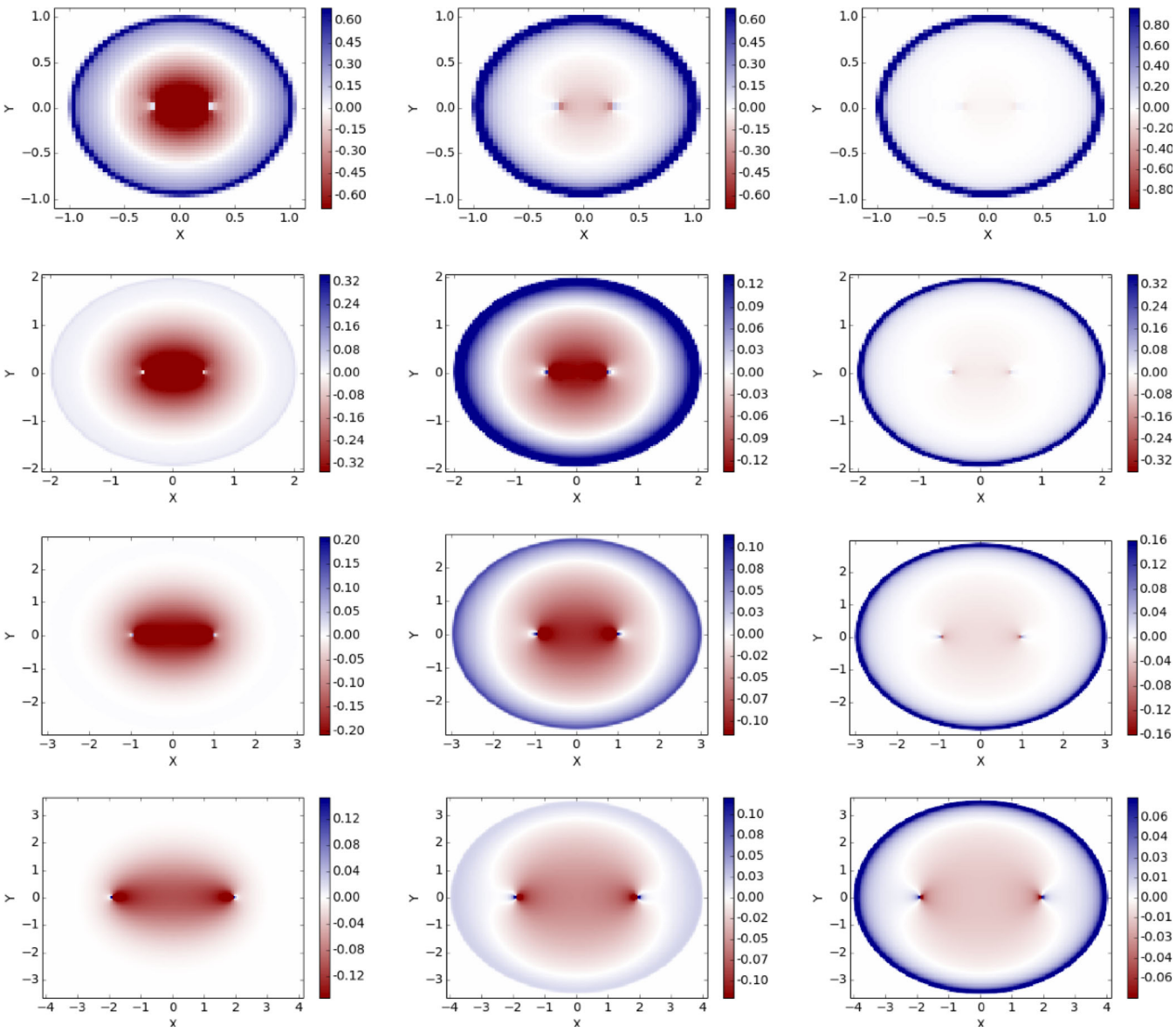

Figure 7. Intensity sensitivity kernels of coda waves for scattering perturbations. The scattering anisotropy increases from left to right $g = 0$, 0.67, 0.9. For each value of g, the kernels have been normalized by the total spatial sensitivity. The four rows correspond to the following epicentral distance and lapse time in the coda (from top to bottom): $R = 0.48l$, $t = 2\tau_s$; $R = 0.96l$, $t = 4\tau_s$; $R = 1.92l$, $t = 6\tau_s$; $R = 3.84l$, $t = 8\tau_s$. To facilitate the visualization, the colour scale has been saturated by clipping all values larger than one-third the maximal sensitivity.

kernel $K_{\rm dc}$. Based on this energy balance, we conclude that the perturbation of intensity caused by a perturbation of scattering properties in $dV(\mathbf{r}')$ at time t in the coda can be expressed as:

$$\frac{\delta I}{I}(dV(\mathbf{r}'), t; \mathbf{r}, \mathbf{r}_0) = \omega \delta Q_{\rm sc}^{-1}(\mathbf{r}') K_{\rm sc}(\mathbf{r}', t; \mathbf{r}, \mathbf{r}_0) dV(\mathbf{r}'), \tag{44}$$

where the intensity sensitivity function for scattering perturbations is simply the difference between the active and passive kernels:

$$K_{\rm sc}(\mathbf{r}', t; \mathbf{r}, \mathbf{r}_0) = K_{\rm dc}(\mathbf{r}', t; \mathbf{r}, \mathbf{r}_0) - K_{tt}(\mathbf{r}', t; \mathbf{r}, \mathbf{r}_0) \tag{45}$$

The result (45) has been established using a perturbative approach by Mayor *et al.* (2014). These authors also demonstrate that eq. (45) implies conservation of energy, which means that integrating the kernel $K_{\rm sc}$ over all detection points $\mathbf{r}$ gives 0. In this work, we have employed basic physical reasoning to recover these results.

In Fig. 7, we illustrate the impact of anisotropic scattering on the intensity sensitivity function $K_{\rm sc}$. The reference isotropic case ($g = 0$) is shown on the left, moderate anisotropy is considered in the centre ($g = 2/3$) and strong anisotropy ($g = 9/10$) on the right. The epicentral distance R and lapse time t in the coda increase from top to bottom as before: $R = 0.48l$, $t = 2\tau_s$; $R = 0.96l$, $t = 4\tau_s$; $R = 1.92l$, $t = 6\tau_s$; $R = 3.84l$, $t = 8\tau_s$. The spatial grid employed to discretize the kernel is the same as in Figs 5 and 6 and the kernels have been normalized by

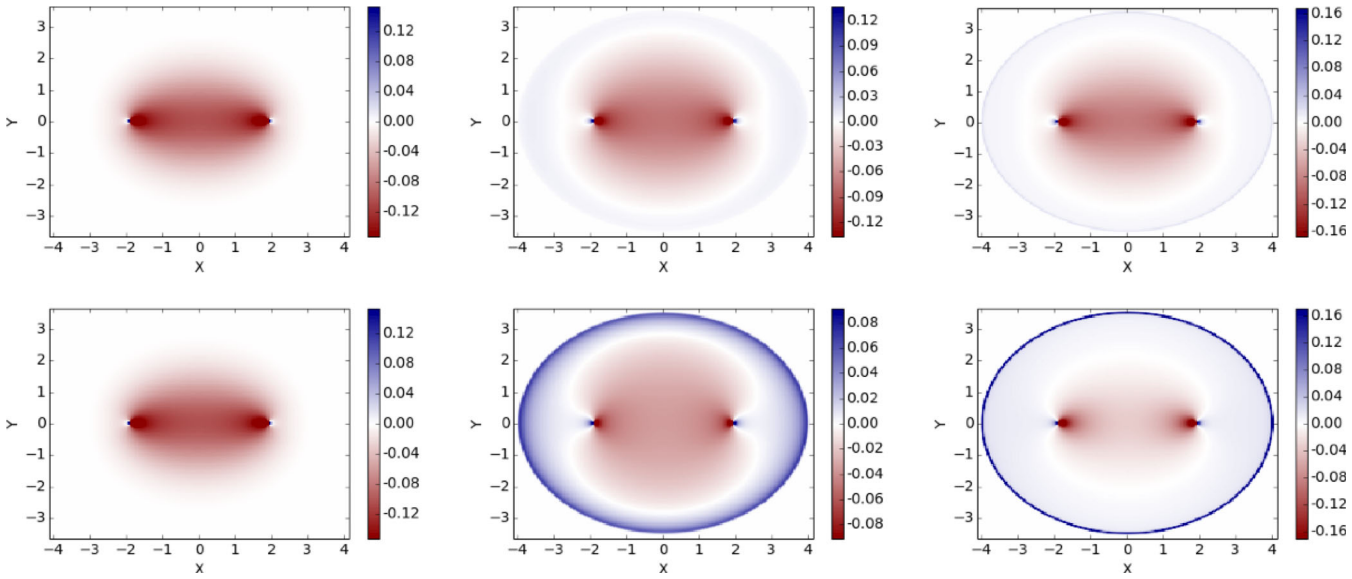

Figure 8. Comparison of isotropic (left), anisotropic (centre) and isotropic-equivalent (right) intensity kernels for scattering perturbations (see the text for a definition of 'isotropic-equivalent'). The top and bottom plots correspond to weak ($g = 0.5$) and moderate ($g = 0.8$) anisotropic scattering, respectively.

the integral of their absolute value. The singularities at the source, receiver and in the vicinity of the single-scattering ellipse are clearly visible in Fig. 7 but the detailed pattern of sensitivity is rather complex. The most prominent effect of scattering anisotropy is to strongly accentuate the positive sensitivity in the vicinity of the single-scattering ellipse, and to considerably reduce the sensitivity to scattering perturbations in the bulk of the medium. The sensitivity on the single-scattering ellipse starts to decrease notably at a lapse time greater than the transport mean-free time, which corresponds to the destruction of the ballistic peak behind the coherent wave (see 'Decorrelation sensitivity kernels' in Section 5). We also observe that the overall shape of the kernel is strongly affected by the level of scattering anisotropy. In the isotropic case, we remark that for a lapse time typically greater than 4 mean-free times, the kernel is dominated by a zone of negative sensitivity distributed along the direct ray path of typical width one mean-free path. Anisotropic scattering modifies this picture in two ways. First, we observe that in addition to a zone of negative sensitivity located in between the two stations, an area of strong positive sensitivity persists in the vicinity of the single-scattering ellipse at longer lapse time ($t \geq 4\tau_s$). This effect is all the more pronounced as the scattering anisotropy increases. Second, we remark that the zone of negative sensitivity is itself affected by scattering anisotropy. In particular, the diffuse–diffuse contribution is much more homogeneously distributed in the bulk of the medium in the anisotropic case than in the isotropic one, as a consequence of the faster diffusion of the waves in the medium. This effect was previously noted in the last two sections.

It is well established that at sufficiently long lapse time—typically larger than the transport mean-free time—, energy transport in an anisotropically scattering medium can be well modeled by an isotropic multiple-scattering process (see e.g. Sheng 2006, for details). Therefore, as a conclusion to this section, we briefly examine the possibility to approximate the intensity sensitivity kernel for anisotropic scattering, by an equivalent isotropic sensitivity kernel with mean-free time $\tau^* = \tau_s/(1-g)$. In the last equation, τ_s and g refer to the mean-free time and mean cosine of the scattering angle in the anisotropic scattering medium. The change of temporal scale $\tau_s \to \tau^*$ in the isotropic approximation guarantees that the two processes share the same asymptotic diffusive behaviour. It is worth noting that the substitution $\tau_s \to \tau^*$ does not correctly rescale the coherent part of the intensity, which decays at a rate controlled by the mean-free path τ_s (see eq. 22), independent of the fact that scattering is isotropic or not. It would be tempting to use two different timescales (τ_s for the coherent intensity, τ^* for the diffuse intensity) but this ad-hoc procedure would violate the conservation of energy. As a consequence, the sensitivity in the vicinity of the source always differs between the anisotropic model and its isotropic approximation. In Fig. 8, we compare the exact intensity sensitivity kernel for anisotropic scattering (centre) with the approximate kernel (right) based on the equivalent isotropic multiple-scattering process defined above. For reference, we also show the sensitivity kernel for isotropic scattering with mean-free time τ_s (and not τ^*). Two cases with respectively weak ($g = 0.5$, top) and moderate anisotropy ($g = 0.8$, bottom) are considered for one epicentral distance $R = 3.84l$ ($R = 1.92l^*$ for $g = 0.5$; $R = 0.768l^*$ for $g = 0.8$) and one lapse time $t = 8\tau_s$ ($t = 4\tau^*$ for $g = 0.5$; $t = 1.6\tau^*$ for $g = 0.8$). In the two cases, we find that the equivalent isotropic kernel (right) bears similarities with its exact anisotropic counterpart centre, in particular in comparison with the isotropic kernel obtained without rescaling (left). We remark that the equivalent isotropic kernel displays extra sensitivity on the causality ellipse. This may be traced back to the substitution $\tau_s \to \tau^*$ which overestimates the intensity of the coherent term in the isotropic approximation. In the anisotropic multiple-scattering process, the coherent waves are converted into diffuse which results in a smearing of the kernel near the causality ellipse. In future work, it would be interesting to further quantify the error incurred by the use of the isotropic approximation to image temporal changes in the medium.

7 CONCLUSIONS AND OUTLOOK

In this work, we have carefully studied the effect of scattering anisotropy on the sensitivity kernels for coda-wave interferometry and scattering tomography. We have shown that each observable necessitates an appropriate sensitivity function and have discussed the relations with previous works. In the diffusion regime our theory confirms that a single sensitivity function for traveltime and decorrelation of coda waves may be employed as first shown by Planès *et al.* (2014) based on a diagrammatic approach. The results of geometrical optics and single-scattering theory are recovered as limiting cases of our approach in the case of traveltime or intensity measurements. In the general situation, our results indicate that an estimation of the amount of scattering anisotropy is necessary to correctly predict the effect of spatial (respectively temporal) variations of scattering properties on the intensity of coda waves (resp. decorrelation of coda waves). Such an estimate may be obtained through the direct modeling of the envelope shape of the ballistic pulse in the time domain (Hoshiba 1995; Gusev & Abubakirov 1996), by an analysis of the delay time between onset and maximum of the seismogram envelope (Saito *et al.* 2005; Takahashi *et al.* 2009), or by a modeling of the lapse-time dependence of the coda quality factor Q_c (Calvet & Margerin 2013). This implies that the effect of scattering anisotropy can be incorporated in the modeling of coda-wave sensitivity functions but requires an extra step compared to the isotropic case. Our results have direct implications for imaging applications. Interestingly, the method of Nishigami (2000)—a form of migration technique for scattering anomalies in the crust—, which assumes that the sensitivity of the coda is concentrated on the single-scattering ellipse may be well founded in the presence of strong anisotropic scattering in the crust, as illustrated in Fig. 7. In monitoring applications based on traveltime changes in the coda, a simplified sensitivity function has often been employed, which concentrates the sensitivity on the direct ray path. Such an approximation may work very well if scattering is isotropic and sufficiently strong (see Fig. 5), as appears to be the case in volcanoes. In absorption/scattering tomography, other approximate treatments emphasizing the sensitivity on the ray path have recently been employed (Prudencio *et al.* 2013, 2015). In the future, our work may facilitate the implementation of more accurate coda-wave sensitivity functions, thereby improving the spatial resolution of current techniques. As it stands, our theory may be useful in cases where the propagation is effectively 2-D, as for example when the signal is dominated by Rayleigh waves. There is still an important need to clarify the depth-sensitivity of coda waves as a function of lapse time. The analysis of Obermann *et al.* (2013b) based on numerical simulations of the waveform provides an interesting perspective on this issue. The problem of imaging temporal changes in media that are not statically homogeneous has not been considered in our study either. In a recent paper, Kanu & Snieder (2015) have tackled this interesting issue using numerically simulated scattered wavefields. In future works, we plan to extend our approach to 3-D anisotropically scattering media in order to clarify the depth-dependent sensitivity of body waves to medium changes.

ACKNOWLEDGEMENTS

This article benefited from the careful reading of an anonymous referee, who suggested several improvements to the original manuscript. The addition of Fig. 8 was suggested by the constructive criticisms of U. Wegler. We acknowledge the financial support of INSU-CNRS through a research grant of the Programme National de Planétologie.

REFERENCES

Aki, K., 1969. Analysis of the seismic coda of local earthquakes as scattered waves, *J. geophys. Res.,* **74,** 615–631.

Aki, K. & Chouet, B., 1975. Origin of coda waves: source, attenuation and scattering effects, *J. geophys. Res,* **80**(23), 3322–3342.

Baddour, N., 2009. Operational and convolution properties of two-dimensional fourier transforms in polar coordinates, *J. Opt. Soc. Am. A,* **26**(8), 1767–1777.

Brenguier, F., Campillo, M., Hadziioannou, C., Shapiro, N., Nadeau, R.M. & Larose, E., 2008a. Postseismic relaxation along the san andreas fault at parkfield from continuous seismological observations, *Science,* **321**(5895), 1478–1481.

Brenguier, F., Shapiro, N.M., Campillo, M., Ferrazzini, V., Duputel, Z., Coutant, O. & Nercessian, A., 2008b. Towards forecasting volcanic eruptions using seismic noise, *Nature Geosci.,* **1**(2), 126–130.

Brenguier, F., Clarke, D., Aoki, Y., Shapiro, N.M., Campillo, M. & Ferrazzini, V., 2011. Monitoring volcanoes using seismic noise correlations, *C. R. Geosci.,* **343**(8), 633–638.

Butz, T., 2006. *Fourier Transformation for Pedestrians,* Springer.

Calvet, M. & Margerin, L., 2013. Lapse-time dependence of coda Q: anisotropic multiple-scattering models and application to the Pyrenees, *Bull. seism. Soc. Am.,* **103**(3), 1993–2010.

Calvet, M., Sylvander, M., Margerin, L. & Villasenõr, A., 2013. Spatial variations of seismic attenuation and heterogeneity in the Pyrenees: coda Q and peak delay time analysis, *Tectonophysics,* **608,** 428–439.

Carcolé, E. & Sato, H., 2010. Spatial distribution of scattering loss and intrinsic absorption of short-period S waves in the lithosphere of Japan on the basis of the Multiple Lapse Time Window Analysis of Hi-net data, *Geophys. J. Int.,* **180**(1), 268–290.

Case, K.M. & Zweifel, P.F., 1967. *Linear Transport Theory,* Addison-Wesley.

Chandrasekhar, S., 1960. *Radiative Transfer,* Dover, New York.

Chen, J., Froment, B., Liu, Q. & Campillo, M., 2010. Distribution of seismic wave speed changes associated with the 12 May 2008 Mw 7.9 Wenchuan earthquake, *Geophys. Res. Lett,* **37,** L18302, doi:10.1029/2010GL044582.

Frankel, A. & Wennerberg, L., 1987. Energy-flux model of seismic coda: separation of scattering and intrinsic attenuation, *Bull. seism. Soc. Am.,* **77**(4), 1223–1251.

Frigo, M. & Johnson, S.G., 2005. The design and implementation of FFTW3, *Proc. IEEE,* **93**(2), 216–231.

Froment, B., Campillo, M., Chen, J. & Liu, Q., 2013. Deformation at depth associated with the 12 May 2008 Mw 7.9 Wenchuan earthquake from seismic ambient noise monitoring, *Geophys. Res. Lett.,* **40**(1), 78–82.

Gradshteyn, I. & Ryzhik, I., 2007. *Table of Integrals, Series and Products,* 7th edn, Academic Press.

Gusev, A.A. & Abubakirov, I.R., 1996. Simulated envelopes of non-isotropically scattered body waves as compared to observed ones: another manifestation of fractal heterogeneity, *Geophys. J. Int.,* **127**(1), 49–60.

Hoshiba, M., 1995. Estimation of nonisotropic scattering in western Japan using coda wave envelopes: application of a multiple nonisotropic scattering model, *J. geophys. Res. (1978–2012),* **100**(B1), 645–657.

Johnson, H.F., 1987. An improved method for computing a discrete Hankel transform, *Comput. Phys. Commun.,* **43**(2), 181–202.

Kanu, C. & Snieder, R., 2015. Time-lapse imaging of a localized weak change with multiply scattered waves using numerical-based sensitivity kernel, *J. geophys. Res.,* **120,** 5595–5605.

Kourganoff, V., 1969. *Introduction to the General Theory of Particle Transfer,* CRC Press.

Larose, E., Planes, T., Rossetto, V. & Margerin, L., 2010. Locating a small change in a multiple scattering environment, *Appl. Phys. Lett.,* **96**(20), 4101, doi:10.1063/1.3431269.

Liemert, A. & Kienle, A., 2011. Radiative transfer in two-dimensional infinitely extended scattering media, *J. Phys. A: Math. Theor.,* **44**(50), 505206, doi:10.1088/1751-113/44/50/505206.

Margerin, L., 2005. Introduction to radiative transfer of seismic waves, in *Seismic Earth: Array Analysis of Broadband Seismograms,* Geophysical Monograph, vol. 157, pp. 229–252, eds Nolet, G. & Levander, A., American Geophysical Union.

Margerin, L. & Nolet, G., 2003. Multiple scattering of high-frequency seismic waves in the deep earth: PKP precursor analysis and inversion for mantle granularity, *J. geophys. Res.,* **108**(B11), 2514, doi:10.1029/2003JB002455.

Margerin, L., Campillo, M. & Van Tiggelen, B., 2000. Monte-Carlo simulation of multiple scattering of elastic waves, *J. geophys. Res.,* **105**(B4), 7873–7892.

Mayor, J., Margerin, L. & Calvet, M., 2014. Sensitivity of coda waves to spatial variations of absorption and scattering: radiative transfer theory and 2-D examples, *Geophys. J. Int.,* **197,** 1117–1137.

Mitchell, B. & Cong, L., 1998. Lg coda *Q* and its relation to the structure and evolution of continents: a global perspective, *Pure appl. Geophys.,* **153,** 655–663.

Nakata, N. & Snieder, R., 2011. Near-surface weakening in Japan after the 2011 Tohoku-Oki earthquake, *Geophys. Res. Lett.,* **38**(17), doi:10.1029/2011GL048800.

Nishigami, K., 2000. Deep crustal heterogeneity along and around the san andreas fault system in central California and its relation to the segmentation, *J. geophys. Res.,* **105**(B4), 7983–7998.

Obermann, A., Planes, T., Larose, E. & Campillo, M., 2013a. Imaging preeruptive and coeruptive structural and mechanical changes of a volcano with ambient seismic noise, *J. geophys. Res.,* **118**(12), 6285–6294.

Obermann, A., Planès, T., Larose, E., Sens-Schönfelder, C. & Campillo, M., 2013b. Depth sensitivity of seismic coda waves to velocity perturbations in an elastic heterogeneous medium, *Geophys. J. Int.,* **194**(1), 372–382.

Paasschens, J., 1997. Solution of the time-dependent Boltzmann equation, *Phys. Rev. E,* **56,** 1135–1141.

Pacheco, C. & Snieder, R., 2005. Time-lapse travel time change of multiply scattered acoustic waves, *J. acoust. Soc. Am.,* **118,** 1300–1310.

Pacheco, C. & Snieder, R., 2006. Time-lapse traveltime change of singly scattered acoustic waves, *Geophys. J. Int.,* **165**(2), 485–500.

Panasyuk, G., Schotland, J.C. & Markel, V.A., 2006. Radiative transport equation in rotated reference frames, *J. Phys. A: Math. Gen.,* **39,** 115–137.

Planès, T., Larose, E., Margerin, L., Rossetto, V. & Sens-Schönfelder, C., 2014. Decorrelation and phase-shift of coda waves induced by local changes: multiple scattering approach and numerical validation, *Waves Random Complex Media,* **24**(2), 99–125.

Planès, T., Larose, E., Rossetto, V. & Margerin, L., 2015. Imaging multiple local changes in heterogeneous media with diffuse waves, *J. acoust. Soc. Am.,* **137,** 660–667.

Prudencio, J., Del Pezzo, E., García-Yeguas, A. & Ibáñez, J.M., 2013. Spatial distribution of intrinsic and scattering seismic attenuation in active volcanic islands—I: model and the case of Tenerife Island, *Geophys. J. Int.,* **195**(3), 1942–1956.

Prudencio, J., Del Pezzo, E., Ibáñez, J.M., Giampiccolo, D. & Patané, D., 2015. Two-dimensional seismic attenuation images of Stromboli Island using active data, *Geophys. Res. Lett.,* **42,** doi:10.1002/2015GL063293.

Saito, T., Sato, H., Ohtake, M. & Obara, K., 2005. Unified explanation of envelope broadening and maximum-amplitude decay of high-frequency seismograms based on the envelope simulation using the Markov approximation: forearc side of the volcanic front in northeastern Honshu, Japan, *J. geophys. Res.,* **110,** B01304, doi:10.1029/2004JB003225.

Sato, H., 1994. Formulation of the multiple non-isotropic scattering process in 2-d space on the basis of energy-transport theory, *Geophys. J. Int.,* **117**(3), 727–732.

Sato, H., Fehler, M.C. & Maeda, T., 2012. *Seismic Wave Propagation and Scattering in the Heterogeneous Earth,* vol. 496, Springer.

Sens-Schönfelder, C. & Wegler, U., 2006. Passive image interferometry and seasonal variations of seismic velocities at Merapi Volcano, Indonesia, *Geophys. Res. Lett.,* **33,** L21302, doi:10.1029/2006GL027797.

Sens-Schönfelder, C. & Wegler, U., 2011. Passive image interferometry for monitoring crustal changes with ambient seismic noise, *C. R. Geosci.,* **343**(8), 639–651.

Sens-Schönfelder, C., Pomponi, E. & Peltier, A., 2014. Dynamics of Piton de la Fournaise volcano observed by passive image interferometry with multiple references, *J. Volc. Geotherm. Res.,* **276,** 32–45.

Shang, T. & Gao, L., 1988. Transportation theory of multiple scattering and its application to seismic coda waves of impulsive source, *Sci. Sin.,* **31,** 1503–1514.

Shearer, P.M. & Earle, P.S., 2004. The global short-period wavefield modelled with a Monte Carlo seismic phonon method, *Geophys. J. Int.,* **158**(3), 1103–1117.

Sheng, P., 2006. *Introduction to Wave Scattering, Localization and Mesoscopic Phenomena,* Springer Science & Business Media.

Snieder, R., 2006. The theory of coda wave interferometry, *Pure appl. Geophys.,* **163**(2–3), 455–473.

Takahashi, T., Sato, H., Nishimura, T. & Obara, K., 2009. Tomographic inversion of the peak delay times to reveal random velocity fluctuations in the lithosphere: method and application to northeastern Japan, *Geophys. J. Int.,* **178**(3), 1437–1455.

Wegler, U. & Sens-Schönfelder, C., 2007. Fault zone monitoring with passive image interferometry, *Geophys. J. Int.,* **168**(3), 1029–1033.

Yamamoto, M. & Sato, H., 2010. Multiple scattering and mode conversion revealed by an active seismic experiment at Asama volcano, Japan, *J. geophys. Res.,* **115**(B7), B07304, doi:10.1029/2009JB007109.

Yu, T.-C. & Hung, S.-H., 2012. Temporal changes of seismic velocity associated with the 2006 Mw 6.1 Taitung earthquake in an arc-continent collision suture zone, *Geophys. Res. Lett.,* **39**(12), doi:10.1029/2012GL051970.